Coordination Algorithms Control Molecular Architecture: $[Cu^{I}_4(L2)_4]^{4+}$ Grid Complex Versus $[M^{II}_2(L2)_2X_4]^{y+}$ Side-By-Side Complexes (M = Mn, Co, Ni, Zn; X = Solvent or Anion) and $[Fe^{II}(L2)_3][Cl_3Fe^{III}OFe^{III}Cl_3]$

Yanhua Lan,[a] Dietmar K. Kennepohl,[a, b] Boujemaa Moubaraki,[c] Keith S. Murray,[c] John D. Cashion,[d] Geoffrey B. Jameson,[e] and Sally Brooker*[a]

Abstract: The synthesis and characterisation of a pyridazine-containing two-armed grid ligand L2 (prepared from one equivalent of 3,6-diformylpyridazine and two equivalents of *p*-anisidine) and the resulting transition metal (Zn, Cu, Ni, Co, Fe, Mn) complexes (**1**–**9**) are reported. Single-crystal X-ray structure determinations revealed that the copper(I) complex had self-assembled as a [2 × 2] grid, $[Cu^{I}_4(L2)_4][PF_6]_4\cdot(CH_3CN)(H_2O)(CH_3CH_2OCH_2CH_3)_{0.25}$ (**2**$\cdot(CH_3CN)(H_2O)(CH_3CH_2OCH_2CH_3)_{0.25}$), whereas the $[Zn_2(L2)_2(CH_3CN)_2(H_2O)_2][ClO_4]_4\cdot CH_3CN$ (**1**$\cdot CH_3CN$), $[Ni^{II}_2(L2)_2(CH_3CN)_4][BF_4]_4\cdot(CH_3CH_2OCH_2CH_3)_{0.25}$ (**5a**$\cdot(CH_3CH_2OCH_2CH_3)_{0.25}$) and $[Co^{II}_2(L2)_2(H_2O)_2(CH_3CN)_2][ClO_4]_4\cdot(H_2O)(CH_3CN)_{0.5}$ (**6a**$\cdot(H_2O)(CH_3CN)_{0.5}$) complexes adopt a side-by-side architecture; iron(II) forms a monometallic cation binding three L2 ligands, $[Fe^{II}(L2)_3][Fe^{III}Cl_3OCl_3Fe^{III}]\cdot CH_3CN$ (**7**$\cdot CH_3CN$). A more soluble salt of the cation of **7**, the diamagnetic complex $[Fe^{II}(L2)_3][BF_4]_2\cdot 2H_2O$ (**8**), was prepared, as well as two derivatives of **2**, $[Cu^{I}_2(L2)_2(NCS)_2]\cdot H_2O$ (**3**) and $[Cu^{I}_2(L2)(NCS)_2]$ (**4**). The manganese complex, $[Mn^{II}_2(L2)_2Cl_4]\cdot 3H_2O$ (**9**), was not structurally characterised, but is proposed to adopt a side-by-side architecture. Variable temperature magnetic susceptibility studies yielded small negative J values for the side-by-side complexes: $J = -21.6$ cm^{-1} and $g = 2.17$ for $S = 1$ dinickel(II) complex $[Ni^{II}_2(L2)_2(H_2O)_4][BF_4]_4$ (**5b**) (fraction monomer 0.02); $J = -7.6$ cm^{-1} and $g = 2.44$ for $S = 3/2$ dicobalt(II) complex $[Co^{II}_2(L2)_2(H_2O)_4][ClO_4]_4$ (**6b**) (fraction monomer 0.02); $J = -3.2$ cm^{-1} and $g = 1.95$ for $S = 5/2$ dimanganese(II) complex **9** (fraction monomer 0.02). The double salt, mixed valent iron complex **7**$\cdot H_2O$ gave $J = -75$ cm^{-1} and $g = 1.81$ for the $S = 5/2$ diiron(III) anion (fraction monomer = 0.025). These parameters are lower than normal for $Fe^{III}OFe^{III}$ species because of fitting of superimposed monomer and dimer susceptibilities arising from trace impurities. The iron(II) centre in **7**$\cdot H_2O$ is low spin and hence diamagnetic, a fact confirmed by the preparation and characterisation of the simple diamagnetic iron(II) complex **8**. Mössbauer measurements at 77 K confirmed that there are two iron sites in **7**$\cdot H_2O$, a low-spin iron(II) site and a high-spin diiron(III) site. A full electrochemical investigation was undertaken for complexes **1**, **2**, **5b**, **6b** and **8** and this showed that multiple redox processes are a feature of all of them.

Keywords: bridging ligands · electrochemistry · ligand design · magnetochemistry · self-assembly

[a] Dr. S. Brooker, Y. Lan, Prof. D. K. Kennepohl
Department of Chemistry, University of Otago
P.O. Box 56, Dunedin (New Zealand)
Fax: (+64) 3-479-7906
E-mail: sbrooker@alkali.otago.ac.nz

[b] Prof. D. K. Kennepohl
Centre for Science, Athabasca University
1 University Drive, Athabasca, Alberta, T9S 3A3 (Canada)

[c] Dr. B. Moubaraki, Prof. K. S. Murray
School of Chemistry, Monash University
P.O. Box 23, Clayton, Victoria 3800 (Australia)

[d] Dr. J. D. Cashion
School of Physics and Materials Engineering, Monash University
P.O. Box 27, Victoria 3800 (Australia)

[e] Prof. G. B. Jameson
Institute of Fundamental Sciences, Chemistry
Massey University, P.O. Box 11222
Palmerston North (New Zealand)

Introduction

The prospect of complex supramolecular architectures being self-assembled from *simple* components by careful design of those components is generating much interest and consequently attracting many researchers into this challenging area.[1–4] Recently a [2 × 2] grid complex was self-assembled from copper(I) ions and the Schiff base macrocycle obtained from the [2+2] condensation of 3,6-diformylpyridazine[5–7] and 1,3-diaminopropane (L1).[4] This macrocycle, L1, allowed the isolation of a wide range of transition metal complexes with intriguing properties, in particular redox and magnetic properties.[4, 7–15] In addition to our studies of such macrocyclic complexes, we are examining the expression[1] of related, carefully designed/programmed, polydentate *acyclic* ligands, derived from 3,6-diformylpyridazine[7, 11] and related hetero-

  DOI: 10.1002/chem.200304915

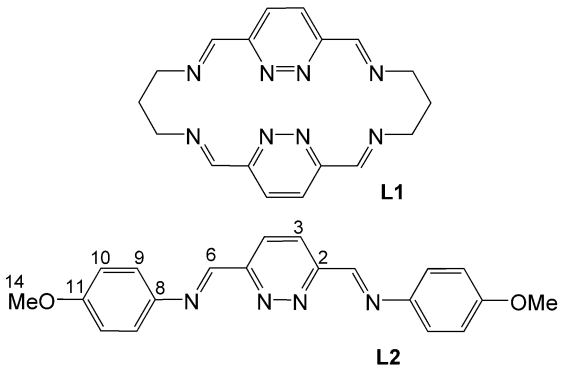

cycles, with appropriate metal ions.[16] One aim of these studies is to explore further the possibilities of self-assembling large supramolecular structures, in particular grids,[3] from readily tuneable Schiff base ligands (e.g., ligand substituents and, hence, electronic and steric properties can be easily varied).[4, 13, 15, 17–19] This paper concerns a system that was designed to produce one or other of two different outcomes, grid and side-by-side architectures (Scheme 1). We report

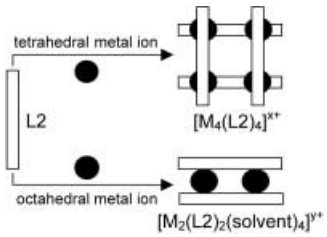

Scheme 1.

here on the results of expression of the programmed ligand system, bis-bidentate L2 (formed from 3,6-diformylpyridazine and *p*-anisidine in 93% yield), with two different metal ion algorithms, metals with four-connecting (tetrahedral) nodes, Cu^{I}, and six-connecting (octahedral) nodes, M^{II} (M = Zn, Ni, Co, Fe, Mn).

Results and Discussion

Synthesis: The ligand L2 ($H_3COPhN{=}CHC_4H_2N_2CH{=}NPhOCH_3$) is prepared from one equivalent of 3,6-diformylpyridazine and two equivalents of *p*-anisidine in reagent grade ethanol, in excellent yield. Even though ligand L2 is only partially soluble in acetonitrile, it readily reacts with all of the transition metal salts in this solvent at room temperature. Complexes **1**, **5**, **6** and **9** were prepared in air, whereas the other complexes **2**–**4**, **7** and **8** were prepared under a nitrogen or argon atmosphere.

All complexes were obtained in excellent yield by reacting one equivalent of ligand L2 with one equivalent of the corresponding metal salt, except for complex **8** which was prepared from three equivalents of ligand L2 and one equivalent of $Fe[BF_4]_2 \cdot 6H_2O$. Complexes **1**, **2**, **5** and **6** were obtained as single crystals by diethyl ether vapour diffusion into the respective reaction solutions in acetonitrile, whereas complex **7** was obtained as single crystals by diethyl ether vapour diffusion into the filtrate of the reaction mixture. The above crystals were characterised by X-ray crystallography (see later). Complex $\mathbf{2} \cdot (CH_3CN)(H_2O)(CH_3CH_2OCH_2CH_3)_{0.25}$ crystallised as dark brown needle-like crystals in which a [2 × 2] grid architecture, similar to that found for the macrocyclic copper(I) complex $[Cu^{I}_4(L1)_2]^{4+}$,[4, 13] is observed (Figure 1). Complex $\mathbf{1} \cdot CH_3CN$ crystallised as orange needles in which a side-by-side architecture is observed (Figure 2). Complexes $\mathbf{5a} \cdot (CH_3CH_2OCH_2CH_3)_{0.25}$ and $\mathbf{6a} \cdot (H_2O)(CH_3CN)_{0.5}$ also have side-by-side architectures (Figures 3 and 4) and were isolated as red blocks and red rods respectively.

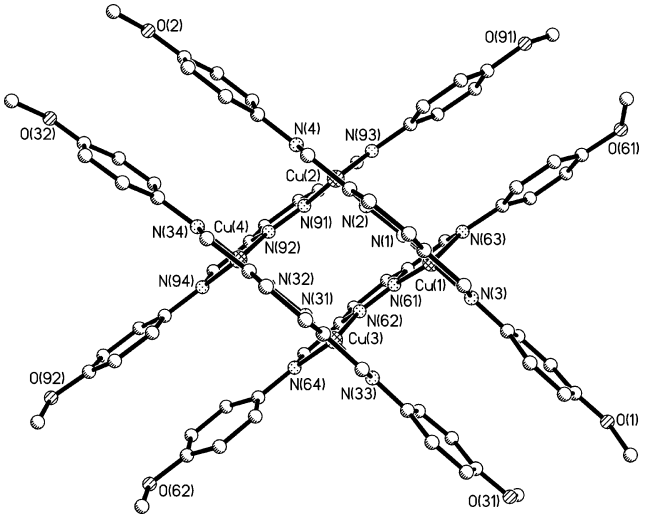

Figure 1. Perspective view of the cation of $\mathbf{2} \cdot (CH_3CN)(H_2O)(CH_3CH_2OCH_2CH_3)_{0.25}$. Selected interatomic distances [Å] and angles [°]: Cu(1)–N(1) 2.012(5), Cu(1)–N(61) 2.014(5), Cu(1)–N(63) 2.038(5), Cu(1)–N(3) 2.056(5), Cu(2)–N(2) 2.004(4), Cu(2)–N(91) 2.011(5), Cu(2)–N(4) 2.043(5), Cu(2)–N(93) 2.042(5), Cu(3)–N(62) 1.960(4), Cu(3)–N(31) 1.969(5), Cu(3)–N(33) 2.040(4), Cu(3)–N(64) 2.051(5), Cu(4)–N(92) 1.992(4), Cu(4)–N(32) 2.014(4), Cu(4)–N(34) 2.050(4), Cu(4)–N(94) 2.069(5), Cu(1)···Cu(2) 3.747(1), Cu(1)···Cu(3) 3.656(1), Cu(1)···Cu(4) 5.681(1), Cu(2)···Cu(3) 4.751(1), Cu(2)···Cu(4) 3.723(1), Cu(3)···Cu(4) 3.687(1), N(1)-Cu(1)-N(61) 123.03(19), N(1)-Cu(1)-N(63) 129.3(2), N(61)-Cu(1)-N(63) 80.9(2), N(1)-Cu(1)-N(3) 81.0(2), N(61)-Cu(1)-N(3) 131.2(2), N(63)-Cu(1)-N(3) 118.3(2), N(2)-Cu(2)-N(91) 133.15(18), N(2)-Cu(2)-N(4) 81.67(18), N(91)-Cu(2)-N(4) 117.90(19), N(2)-Cu(2)-N(93) 121.67(19), N(91)-Cu(2)-N(93) 81.6(2), N(4)-Cu(2)-N(93) 127.46(19), N(62)-Cu(3)-N(31) 132.66(19), N(62)-Cu(3)-N(33) 123.59(19), N(31)-Cu(3)-N(33) 81.72(18), N(62)-Cu(3)-N(64) 81.7(2), N(31)-Cu(3)-N(64) 119.09(19), N(33)-Cu(3)-N(64) 124.05(19), N(92)-Cu(4)-N(32) 127.41(18), N(92)-Cu(4)-N(34) 127.27(18), N(32)-Cu(4)-N(34) 80.77(17), N(92)-Cu(4)-N(94) 80.71(19), N(32)-Cu(4)-N(94) 133.58(18), N(34)-Cu(4)-N(94) 112.97(18).

The reaction of a deep brown solution of $[Cu^{I}_4(L2)_4][BF_4]_4$ in acetonitrile with four equivalents of thiocyanate anions led to the precipitation of **3**, as greenish brown powder, directly from the reaction mixture in high yield. Similarly, complex **4** precipitated directly from a mixture of one equivalent of ligand L2, two equivalents of $[Cu^{I}(CH_3CN)_4]BF_4$ and two equivalents of thiocyanate anions as an intense brown (almost black) powder in high yield. Interestingly, the reaction of L2 with copper(II) tetrafluoroborate in CH_3CN also gave $[Cu^{I}_4(L2)_4][BF_4]_4$, in 60% yield rather than the 89% yield

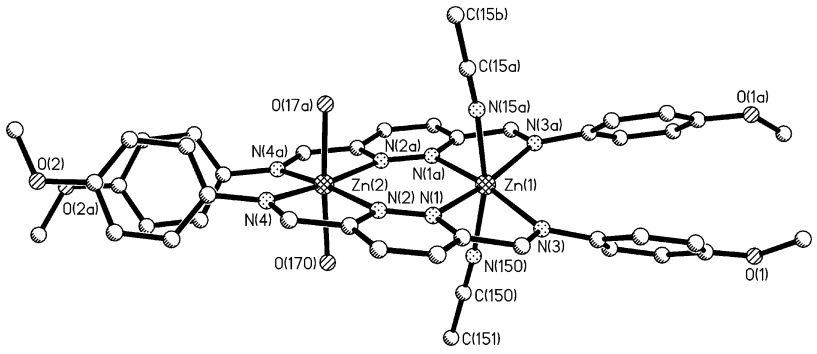

Figure 2. Perspective view of the cation of **1**·CH_3CN. Selected interatomic distances [Å] and angles [°]: Zn(1)–N(3) 2.128(5), Zn(1)–N(150) 2.152(6), Zn(1)–N(1) 2.155(5), Zn(2)–O(170) 2.083(4), Zn(2)–N(4) 2.138(5), Zn(2)–N(2) 2.206(5), Zn(1)···Zn(2) 4.050(4), N(3A)-Zn(1)-N(3) 103.4(3), N(3)-Zn(1)-N(15A) 101.55(18), N(3)-Zn(1)-N(150) 87.09(18), N(15A)-Zn(1)-N(150) 166.1(3), N(3A)-Zn(1)-N(1) 169.11(17), N(3)-Zn(1)-N(1) 77.5(2), N(150)-Zn(1)-N(1) 89.32(18), N(150)-Zn(1)-N(1A) 82.13(18), N(1)-Zn(1)-N(1A) 103.8(3), O(17A)-Zn(2)-O(170) 176.4(2), O(170)-Zn(2)-N(4) 94.17(16), O(170)-Zn(2)-N(4A) 88.01(16), N(4)-Zn(2)-N(4A) 105.1(3), O(170)-Zn(2)-N(2A) 92.02(15), N(4)-Zn(2)-N(2A) 173.46(17), O(170)-Zn(2)-N(2) 85.71(15), N(4)-Zn(2)-N(2) 77.2(2), N(2A)-Zn(2)-N(2) 101.2(3), N(2)-N(1)-Zn(1) 127.9(4), N(1)-N(2)-Zn(2) 128.5(4). Symmetry transformation used to generate equivalent atoms: a = $-x$, y, $-z + ½$.

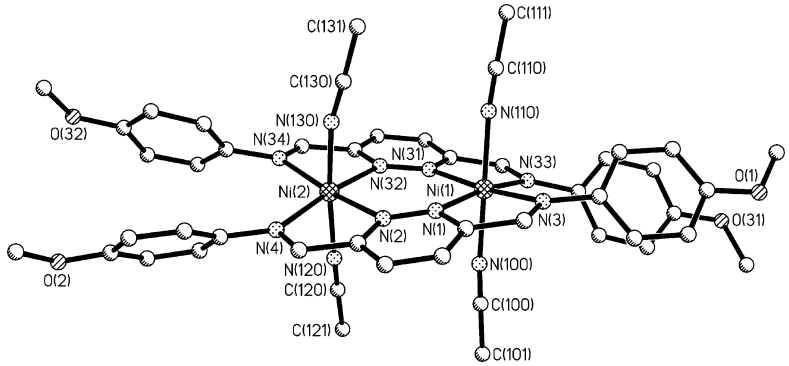

Figure 3. Perspective view of the cation of **5a**·$(CH_3CH_2OCH_2CH_3)_{0.25}$. Selected interatomic distances [Å] and angles [°]: Ni(1)–N(100) 2.029(6), Ni(1)–N(110) 2.072(6), Ni(1)–N(33) 2.136(5), Ni(1)–N(3) 2.138(5), Ni(1)–N(31) 2.146(5), Ni(1)–N(1) 2.159(5), Ni(2)–N(130) 2.042(6), Ni(2)–N(120) 2.065(6), Ni(2)–N(4) 2.130(5), Ni(2)–N(34) 2.134(5), Ni(2)–N(32) 2.154(5), Ni(2)–N(2) 2.155(5), Ni(1)···Ni(2) 4.056(2), N(100)-Ni(1)-N(110) 179.5(2), N(100)-Ni(1)-N(33) 88.1(2), N(110)-Ni(1)-N(33) 91.7(2), N(100)-Ni(1)-N(3) 92.8(2), N(110)-Ni(1)-N(3) 87.7(2), N(33)-Ni(1)-N(3) 102.3(2), N(100)-Ni(1)-N(31) 93.3(2), N(110)-Ni(1)-N(31) 86.2(2), N(33)-Ni(1)-N(31) 78.2(2), N(3)-Ni(1)-N(31) 173.8(2), N(100)-Ni(1)-N(1) 83.3(2), N(110)-Ni(1)-N(1) 96.9(2), N(33)-Ni(1)-N(1) 171.4(2), N(3)-Ni(1)-N(1) 78.7(2), N(31)-Ni(1)-N(1) 101.7(2), N(130)-Ni(2)-N(120) 174.6(2), N(130)-Ni(2)-N(4) 96.1(2), N(120)-Ni(2)-N(4) 88.5(2), N(130)-Ni(2)-N(34) 87.6(2), N(120)-Ni(2)-N(34) 94.3(2), N(4)-Ni(2)-N(34) 101.7(2), N(130)-Ni(2)-N(32) 92.0(2), N(120)-Ni(2)-N(32) 83.4(2), N(4)-Ni(2)-N(32) 171.9(2), N(34)-Ni(2)-N(32) 79.0(2), N(130)-Ni(2)-N(2) 85.1(2), N(120)-Ni(2)-N(2) 93.0(2), N(4)-Ni(2)-N(2) 78.9(2), N(34)-Ni(2)-N(2) 172.7(2), N(32)-Ni(2)-N(2) 101.5(2), N(2)-N(1)-Ni(1) 128.1(4), N(1)-N(2)-Ni(2) 128.4(4).

obtained when a copper(I) salt was employed. This result contrasts with that obtained when Cu^{II} was introduced into the L1 macrocycle: an emerald-green square-pyramidal dicopper(II) complex, $[Cu^{II}_2(L1)(CH_3CN)_2]^{4+}$, resulted in that instance, although it should be noted that on occasions the samples were brown due to the spontaneous formation of traces of highly coloured copper(I) contaminants. The key difference between the reactions of copper(II) with the acyclic ligand L2 and macrocyclic ligand L1 is that in the former a tetrahedral arrangement of the donor atoms, suitable for stabilising copper(I), is readily achievable, whereas this is not the case for the L1 macrocycle; therefore the square-pyramidal copper(II) complex can be isolated when a copper(II) starting material is employed in the transmetallation reaction.[9, 13]

In the case of the iron(II) complexes, the reaction of one equivalent of ligand L2 with one equivalent of iron chloride (no precautions were taken to ensure that this reagent was exclusively iron(II) chloride) gave complex $[Fe^{II}(L2)_3][Cl_3Fe^{III}OFe^{III}Cl_3]\cdot CH_3CN$ (**7**, Figure 5) as an intense green precipitate directly from the reaction mixture. In contrast, the addition of one equivalent of iron(II) tetrafluoroborate to three equivalents of ligand L2 resulted in the crystallisation of complex $[Fe^{II}(L2)_3][BF_4]_2\cdot 2H_2O$ (**8**), as dark green crystals by diethyl ether vapour diffusion into the reaction solution. These reactions demonstrate that the well-known, strong tendency of iron(II) to bind three bidentate nitrogen-heterocycle-based ligands and go low-spin dominates this chemistry, and results in a third, unsurprising, outcome (cf. Scheme 1).

Infrared spectra: Pyridazine ring C–C and C–N stretches (ca. 1593 and 1503 cm^{-1}) as well as a *para*-substituted benzene ring C–H out-of-plane bend (ca. 830 cm^{-1}) are present in the infrared spectra of all of these complexes. The infrared spectrum of L2 exhibits a sharp C=N stretch at 1622 cm^{-1}. There is no evidence of either primary amine stretches (typically 3400–3330 and 3330–3250 cm^{-1}) or a carbonyl stretch (3,6-diformylpyridazine, 1716 cm^{-1}). As expected, the infrared spectra of the complexes **1**–**9** have many similar features. Relative to L2, the C=N stretch occurs at a lower energy in the complexes **2**–**8** (3–18 cm^{-1} lower), whereas for complexes **1** and **9** this stretch occurs at the same position. In addition to the bands due to the presence of L2, the infrared spectra of the non-chloride complexes also contain bands associated with the various anions present. The perchlorate bands observed for complexes **1** and **6b** (at ca. 1120 and 625 cm^{-1}) in both cases show no signs of peak splitting, so the perchlorate ions are not expected to show any significant interactions with the $[Zn_2(L2)_2]^{4+}$ and $[Co_2(L2)_2]^{4+}$ ions. Hexafluorophosphate bands, which are normally observed

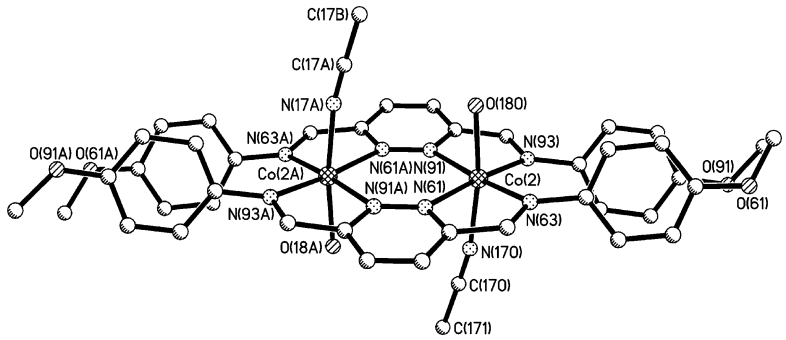

Figure 4. Perspective view of one of the two independent cations of $\mathbf{6a}\cdot(H_2O)(CH_3CN)_{0.5}$. Selected interatomic distances [Å] and angles [°]: Co(2)–O(180) 2.076(3), Co(2)–N(170) 2.105(4), Co(2)–N(93) 2.162(4), Co(2)–N(63) 2.167(5), Co(2)–N(91) 2.192(5), Co(2)–N(61) 2.193(4), Co(2)···Co(2A) 4.066(2), O(180)-Co(2)-N(170) 171.7(2), O(180)-Co(2)-N(93) 93.71(15), N(170)-Co(2)-N(93) 90.19(17), O(180)-Co(2)-N(63) 89.92(16), N(170)-Co(2)-N(63) 96.44(19), N(93)-Co(2)-N(63) 102.55(18), O(180)-Co(2)-N(91) 85.09(16), N(170)-Co(2)-N(91) 88.57(19), N(93)-Co(2)-N(91) 77.39(17), N(63)-Co(2)-N(91) 174.99(14), O(180)-Co(2)-N(61) 91.58(15), N(170)-Co(2)-N(61) 84.56(16), N(93)-Co(2)-N(61) 174.71(15), N(63)-Co(2)-N(61) 77.46(17), N(91)-Co(2)-N(61) 103.08(16). Symmetry transformation used to generate equivalent atoms: $A = 2-x, -y, 1-z$.

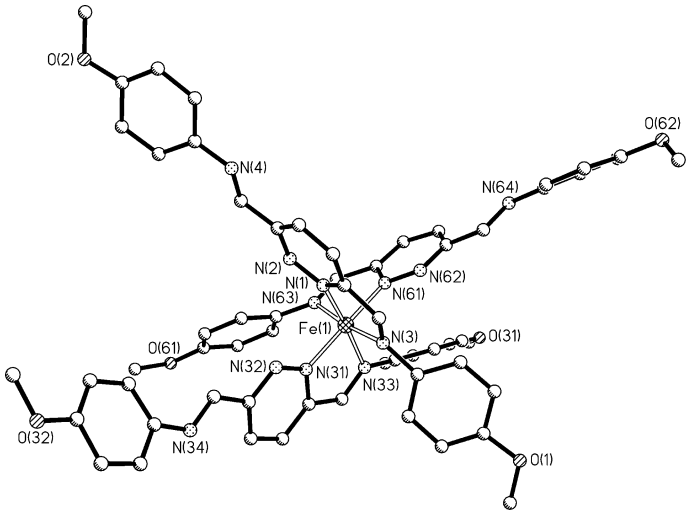

Figure 5. Perspective view of the cation of $\mathbf{7}\cdot CH_3CN$. Selected interatomic distances [Å] and angles [°]: Fe(1)–N(31) 1.911(7), Fe(1)–N(1) 1.933(6), Fe(1)–N(61) 1.941(7), Fe(1)–N(33) 1.984(6), Fe(1)–N(63) 2.004(7), Fe(1)–N(3) 2.009(7), Fe(2)–O(80) 1.767(6), Fe(2)–Cl(2) 2.231(3), Fe(2)–Cl(3), 2.234(4), Fe(2)–Cl(1) 2.240(3), Fe(3)–O(80) 1.740(6), Fe(3)–Cl(5) 2.217(3), Fe(3)–Cl(6) 2.220(3), Fe(3)–Cl(4) 2.233(3), N(31)-Fe(1)-N(1) 95.3(3), N(31)-Fe(1)-N(61) 173.4(3), N(1)-Fe(1)-N(61) 90.0(3), N(31)-Fe(1)-N(33) 80.0(3), N(1)-Fe(1)-N(33) 175.3(3), N(61)-Fe(1)-N(33) 94.7(3), N(31)-Fe(1)-N(63) 95.0(3), N(1)-Fe(1)-N(63) 96.5(3), N(61)-Fe(1)-N(63) 80.5(3), N(33)-Fe(1)-N(63) 84.4(3), N(31)-Fe(1)-N(3) 91.1(3), N(1)-Fe(1)-N(3) 81.3(3), N(61)-Fe(1)-N(3) 93.5(3), N(33)-Fe(1)-N(3) 98.2(3), N(63)-Fe(1)-N(3) 173.7(3), O(80)-Fe(2)-Cl(2) 111.5(3), O(80)-Fe(2)-Cl(3) 109.6(3), Cl(2)-Fe(2)-Cl(3) 107.07(11), O(80)-Fe(2)-Cl(1) 109.5(2), Cl(2)-Fe(2)-Cl(1) 108.34(11), Cl(3)-Fe(2)-Cl(1) 110.86(11), O(80)-Fe(3)-Cl(5) 108.7(2), O(80)-Fe(3)-Cl(6) 110.8(3), Cl(5)-Fe(3)-Cl(6) 110.27(13), O(80)-Fe(3)-Cl(4) 109.9(3), Cl(5)-Fe(3)-Cl(4) 107.85(13), Cl(6)-Fe(3)-Cl(4) 109.21(12), Fe(3)-O(80)-Fe(2) 173.4(4).

at about 840 and 557 cm^{-1},[20] are present in the infrared spectrum of complex **2**, although the first of these, centred at 835 cm^{-1}, is quite broad, presumably due to overlap with the *para*-substituted benzene vibration. In both complexes **3** and **4**, only one thiocyanate stretch is observed, at 2112 cm^{-1}, which indicates that there is just one binding mode for the coordinated thiocyanate ion. The strong absorption at 1083 cm^{-1} and weak absorption at 533 and 521 cm^{-1} for complexes **5b** and **8** are associated with the tetrafluoroborate anions. Because of the interesting counterion $[Cl_3FeOFeCl_3]^{2-}$ in complex $\mathbf{7}\cdot H_2O$, the infrared spectrum was also measured as a KBr disk in the region 200–500 cm^{-1}. Two broad bands are observed at 363 and 314 cm^{-1}, in accord with the observations of Nelson[21] and Wieghardt,[22] and consistent with the observed structure (see later). These authors identified these two bands as being due to a doubly degenerate antisymmetric Cl-Fe-Cl stretch and a symmetric Cl-Fe-Cl stretch, respectively. The other expected broad band, due to the asymmetric Fe-O-Fe stretch at 860–880 cm^{-1},[22] could not be clearly identified owing to the presence of many ligand bands in this region.

UV-visible spectra: UV-visible spectra were recorded for the complexes that had sufficient solubility in acetonitrile, DMF or nitromethane (i.e., all except **4**). These complexes showed an intense absorbance in the range 378–419 nm ($\varepsilon = 39200$–$143300\ dm^3\,mol^{-1}\,cm^{-1}$) due to a charge-transfer transition. In addition, the octahedral high-spin complex **5b** displays a low-intensity absorption at 866 nm ($\varepsilon = 57\ dm^3\,mol^{-1}\,cm^{-1}$), which is associated with the $^3A_{2g} \rightarrow {}^3T_{2g}$ transition. In the case of the low-spin iron(II) complexes there is another broad (81 nm width at half height) and intense charge-transfer band centred at 599 nm ($\varepsilon = 10800$ and $12200\ dm^3\,mol^{-1}\,cm^{-1}$ for complexes $\mathbf{7}\cdot H_2O$ and **8**, respectively) that may well mask the weak d–d absorbances. For the octahedral high-spin complex **6b**, the observation of one weak broad band centred at 921 nm ($\varepsilon = 29\ dm^3\,mol^{-1}\,cm^{-1}$) with a width of ~180 nm is assigned to the $^4T_{1g} \rightarrow {}^4T_{2g}$ transition.

NMR spectra: Simple ^1H and ^{13}C NMR spectra were obtained for L2 and the diamagnetic complexes **1**, **2** and **3** in $CDCl_3$, CD_3CN, CD_3NO_2 and [D_7]DMF, respectively. The fact that, in each of the complexes **1**–**3**, unique signals are observed for just one half of L2 shows that not only are the L2 ligands equivalent to each other, but also that there is two-fold symmetry within the L2 ligand strand. This requires that either the structures observed in the solid state (see later) have increased symmetry in solution or that the complexes are fluxional. Either way these compounds are clearly stable in solution so their formation is not dependent on crystallisation effects. Because of the low solubility of complex **3**, even in DMF, quaternary carbons cannot be seen in the ^{13}C NMR spectrum, due to their long relaxation times.

In contrast, the diamagnetic complex **8** has much more complex ^1H and ^{13}C NMR spectra. The $[Fe^{II}(L2)_3]^{2+}$ species

has no symmetry in the crystal structure (see structure of **7** later) or in solution; where a single signal was observed in the case of ligand L2 and complexes **1**–**3**, six signals are observed in the case of complex **8**. Another consequence of the lack of any symmetry is that the signals corresponding to the hydrogen atoms of the pyridazine ring are now split into doublets.

Mass spectra: All of the complexes fragmented extensively. The electrospray (ES) mass spectrum of **1** showed the successive loss of solvent molecules (CH_3CN or H_2O). The fast atom bombardment (FAB) mass spectrum of **2** had a fragmentation pattern consistent with the successive loss of PF_6 anions and then with the [2 × 2] grid breaking in half. In the electrospray mass spectrum of **3** the fragments were due to the loss of one copper and one L2, followed by loss of one thiocyanate and water. The ES mass spectrum of **5b** revealed only mono-nickel mono-ligand fragments. Likewise, the FAB mass spectrum of **6b** only had fragments corresponding to mono-cobalt species. The ES mass spectra of both of the iron complexes, **7**·H_2O and **8**, had a very clear signal for the doubly charged ion $[Fe(L2)_3]^{2+}$ at 547 *m*/*z*. In the ES mass spectrum of **9** weak signals corresponding to $[Mn_2(L2)_2Cl_3]^+$ and $[Mn(L2)_2Cl]^+$ were clearly observed.

Conductivity: Conductivity measurements were recorded in acetonitrile, DMF or nitromethane for all of the complexes, except for **4** which lacked sufficient solubility in any solvent. The molar conductivity for **1** in acetonitrile is approximately correct for a 4:1 conductor, being somewhat higher than the literature range for a 3:1 electrolyte. The molar conductivities of **2**, **5b**, and **6b** in CH_3CN, all of which are expected to be 4:1 electrolytes, are at the high end of the literature range for 3:1 electrolytes, probably due to the lower mobility of these large cations than those in the simple salts used to determine the literature ranges.[23] The molar conductivity of **3** in DMF is much lower than the literature range for a 1:1 electrolyte, as expected for a nonconductor. The molar conductivity of **7**·H_2O is much lower than the literature range for a 1:1 electrolyte in nitromethane. As expected, **8** in CH_3CN has a molar conductivity value in the literature range for a 2:1 electrolyte. The orange complex **9**, which is expected from the mass spectrum to be a side-by-side complex with octahedral manganese ions, $[Mn_2(L2)_2Cl_4]\cdot 3H_2O$, eventually dissolves in DMF to give a yellow solution, with a molar conductivity somewhat lower than the literature value for a 1:1 electrolyte, indicating that some chloride anions may dissociate on dissolution in DMF.

Structures: The tetracopper(I) complex **2** crystallised, in air, from the acetonitrile reaction solution in 89% yield, by diethyl ether vapour diffusion. The structure determination of **2**·$(CH_3CN)(H_2O)(CH_3CH_2OCH_2CH_3)_{0.25}$ (Figure 1) reveals a similar overall structure to that of $[Cu^I_4(L1)_2]^{4+}$ (ref. [4]) and of the tetracopper(I) grid of the acyclic 3,6-bis(2′-pyridyl)pyridazine (dppn) ligand of Youinou and co-workers.[3a] Each distorted tetrahedral copper(I) centre is coordinated by two almost perpendicular strands of L2 in a [2 × 2] grid arrangement [mean planes through neighbouring pyridazine rings intersect at angles of 102.3° for N(1)/N(61), 101.5° for N(61)/N(31), 103.3° for N(31)/N91), 104.1° for N(91)/N(1)]. Each L2 strand provides two bidentate $N_{imine}N_{pyridazine}$ donor sets to two different copper atoms (bite angle 80.71(19)–81.72(18)°). The pyridazine groups bridge each copper centre to two neighbouring copper centres, forming a rhombus of bridged copper atoms. The pyridazine rings within each almost parallel L2 strand lie over each other and are almost parallel to each other, forming favorable π–π interactions (N(1)/N(31) 0.8° and 3.51–3.56 Å apart, N(61)/N(91) 4.9° and 3.54–3.82 Å apart), as do the phenyl rings (2.5–5.9° and 3.25–3.68 Å apart). Each L2 strand is fairly flat, with mean planes through the phenyl and pyridazine rings intersecting at 9.3–18.5°; this maximises π delocalisation throughout the L2 ligand strand.

Although numerous copper(II) pyridazine-bridged complexes have been reported, copper(I) pyridazine-bridged complexes are less common.[15] The overall [2 × 2] grid architecture of the two most closely related structurally characterised complexes[3a, 4] is compared with that of **2** in Table 1. In the macrocyclic grid complex, $[Cu^I_4(L1)_2]^{4+}$, the Cu_4 moiety is close to square (the adjacent pyridazine rings make internal angles of 90.9–91.9°), with diagonals of almost equal length (although this is also the least planar of these three Cu_4 rings), whereas in the acyclic complexes **2** and $[Cu^I_4(dppn)_4]^{4+}$ the adjacent pyridazine rings form internal angles of about 12° and 22°, respectively, further from orthogonality, and the Cu_4 rings are rhombuses, with diagonals of significantly different lengths (Table 1). This distortion of the orthogonal grid and of the Cu_4 square, to give squashed grids and Cu_4 rhombus cores, is expected to improve the π–π stacking interactions between the almost parallel aromatic rings as it offsets them somewhat.[24]

In marked contrast to the [2 × 2] grid structure that is formed when L2 is expressed with copper(I), when zinc(II), nickel(II) or cobalt(II) ions are used with the same ligand the new coordination algorithm interprets L2 in a different way and produces complexes with a side-by-side architecture,

Table 1. Comparison of some X-ray structural data for complex **2** with two related literature complexes, $[Cu^I_4(L1)_2]^{4+}$ and $[Cu^I_4(dppn)_4]^{4+}$.

Complex	N_{pdz}-Cu-N_{imine}[a] [°]	Cu–N [Å]	∢ pdz ⊥ [b] [°]	∢ pdz ∥ [c] [°]	*d* pdz ∥ [d] [Å]	Cu···Cu[e] [Å]	Ref.
$[Cu^I_4(L1)_2]^{4+}$	79.7–81.7	1.956–2.067	90.9–91.9	0.9, 2.9	3.57–3.72	5.228, 5.310	[4]
$[Cu^I_4(L2)_4]^{4+}$	80.7–81.7	1.960–2.069	101.5–104.1	0.8, 4.9	3.51–3.82	4.751, 5.681	this work
$[Cu^I_4(dppn)_4]^{4+}$	79.9–81.8	1.974–2.041	111.9–114.2	1.2	3.32–3.40	4.533, 5.527	[3a]

[a] Both nitrogen atoms from the same ligand strand. [b] Angles between neighbouring, almost perpendicular pyridazine rings. [c] Angles between opposite, almost parallel pyridazine rings. [d] Distance between opposite, almost parallel pyridazine rings. [e] Across the diagonal of the Cu_4 rhombus.

$[M^{II}_2(L2)_2X_4]^{4+}$ (M = Zn, X_4 = 2 CH_3CN and 2 H_2O **1**; M = Ni, X_4 = 4 CH_3CN **5a**; M = Co, X_4 = 2 CH_3CN and 2 H_2O **6a**).

Crystals of **1**·(CH_3CN), **5a**·$(Et_2O)_{0.25}$ and **6a**·$(H_2O)(CH_3CN)_{0.5}$ were grown from the respective reaction solutions in acetonitrile by diethyl ether vapour diffusion, and X-ray structure determinations were carried out (Figures 2, 3 and 4). The structures are very different from that of the copper(I) complex of the same L2 ligand, despite having the same metal:ligand ratio. The three complexes are similarly self-assembled as side-by-side structures. Here each metal atom (Zn^{2+}, Ni^{2+} and Co^{2+}) is bound by two almost coplanar bidentate $N_{imine}N_{pyridazine}$ moieties from two different L2 strands (bite angle 77.2(2)–77.5(2)° for **1**, 78.2(2)–79.0(2)° for **5a** and 77.04(15)–77.46(17)° for **6a**), and the distorted octahedral geometry is completed by the axial coordination of two solvent molecules, acetonitrile and/or water molecules. There is no crystallographic symmetry within the side-by-side structure of **5a** (dinickel); however, in the cases of **1** (dizinc) and **6a** (dicobalt) the two halves of the side-by-side structures are related by a twofold axis and a centre of inversion, respectively. In all cases, as expected on steric grounds, the two L2 ligand strands are significantly twisted: the pyridazine-ring mean plane within a L2 strand intersects the phenyl-ring mean planes in that strand at 31.4–54.0° for **1**, 39.2–48.6° for **5a** and 42.2–43.1° for **6a**. The extent of π delocalisation within an L2 ligand strand is therefore considerably reduced in these side-by-side complexes relative to that found in the grid complex, **2**. The phenyl rings within the side-by-side L2 strands lie over each other, and are almost parallel to each other, forming favorable π–π interactions (4.7–10.0° and 3.01–3.47 Å apart for **1**, 9.3–21.3° and 2.98–4.02 Å apart for **5a** and 9.3–9.9° and 2.98–3.49 Å apart for **6a**). These appear to be more favourable than those formed in the copper(I) grid complex **2**, and this presumably offsets the effect of the loss of π delocalisation within the individual, twisted, L2 ligand strands in these side-by-side architectures. In addition, these interactions are likely to be important in favouring the formation of these side-by-side architectures as opposed to dimetallic complexes of a single L2 ligand strand.

In contrast to the large volume of literature relating to copper(II) pyridazine complexes,[15] very little attention has been given to the zinc, nickel and cobalt chemistry of such ligands. Only one example of a structurally characterised pyridazine or phthalazine bridged zinc complex has been reported, $[Zn_2(OH)(H_2O)(bdptz)(H_2O)_2]^{3+}$ in which bdptz = 1,4-bis(2,2′-dipyridylmethyl)phthalazine.[25] In that case the two zinc ions are bridged by a single phthalazine bridge, a hydroxide ion and, uncommonly for zinc(II) complexes, a water molecule. The two one-atom bridges lead to a short Zn···Zn separation of 3.169(2) Å relative to the much greater value, 4.050(4) Å, observed in **1**, the first doubly pyridazine bridged zinc complex.

Twenty pyridazine- or phthalazine-bridged nickel complexes have been structurally characterised, of which only six contain doubly diazine bridged nickel ions,[26–31] one of which contains an additional one-atom NCS^- bridge.[31] Of the other five nickel(II) complexes,[26–30] with similar side-by-side structures to that of **5a**, the Ni···Ni separations are in the range 3.791–3.920 Å for those containing octahedral nickel(II) ions,[26, 27, 29] and in the significantly lower range 3.587–3.627 Å for those containing one square planar and one octahedral nickel(II) ion.[28] No details are reported for the last of these structures and the data have not been deposited in the CCDC.[30] The Ni···Ni separation in **5a**, 4.056(2) Å, is somewhat greater than the values reported for these related octahedral nickel(II) complexes.

Other than our own work,[10, 12, 14, 32, 33] there are four structurally characterised cobalt pyridazine/phthalazine complexes in the literature,[34–37] only two of which are of cobalt in the +2 oxidation state.[34, 35] In both of these complexes, one mononuclear and the other dinuclear, the cobalt(II) ions are high spin. In the dinuclear complex, $[Co^{II}_2(PHP6Me)Cl(H_2O)_4]^{3+}$ in which PHP6Me is 1,4-bis[(6-methylpyridine-2-carboxaldimino)amino]phthalazine, the single diazine bridges the two six-coordinate cobalt(II) centres, as does the chloride ion.[34] The presence of the single-atom chloride bridge leads to a shorter Co···Co separation, 3.7121(16) Å, than is the case in **6a**. The double, two-atom pyridazine bridge leads to very similar M···M separations in this series of side-by-side cobalt(II) **6a**, zinc(II) **1** and nickel(II) **5a** complexes of L2 (4.066(2), 4.050(4) and 4.056(2) Å, respectively). In contrast, the series of doubly pyridazine-bridged dicobalt(II) complexes, $[Co^{II}_2(L1)X_4]^{y+}$, that we reported have Co···Co separations in the range 3.750–3.813 Å, and have been high-spin, low-spin or spin-crossover complexes depending on the nature of X.[10, 12, 14] Clearly the macrocyclic nature of the L1 ligand plays a role in constraining the metal-ion geometry relative to that observed in the case of the acyclic ligand L2.

Crystals of **7**·CH_3CN were grown by diethyl ether vapour diffusion into an acetonitrile reaction filtrate and the X-ray crystal structure determined (Figure 5). The stucture is totally different from those of the above complexes, which formed as expected by expression of the L2 ligand with appropriately chosen metal ions (Scheme 1), and represents a third outcome. Here an iron(II) atom is bound by three bidentate $N_{imine}N_{pyridazine}$ moieties from three different L2 strands, and is in a distorted octahedral environment, with angles subtended at the iron(II) centre varying from 80.0(3) to 98.2(3)°. There are no significant differences in the Fe–$N_{pyridazine}$ bond lengths (1.911(7)–1.941(7) Å) or in the Fe–N_{imine} bond lengths (1.984(6)–2.009(7) Å); however, the bond lengths of Fe–$N_{pyridazine}$ are slightly shorter than those of Fe–N_{imine}. These Fe–$N_{pyridazine}$ distances are also short in comparison with the average low-spin Fe^{II}–N bond lengths observed for the related complexes $[Fe^{II}(3,3'\text{-bipyridazine})_3][ClO_4]_2$, $[Fe^{II}(bpy)_3][Cl_3Fe^{III}OFe^{III}Cl_3]$ and $[Fe^{II}(phen)_3][Cl_3Fe^{III}OFe^{III}Cl_3]$, of 1.927(3),[38] 1.97(1)[39] and 1.96(2) Å,[40] respectively. The Fe–N_{imine} bond lengths are slightly longer than these low-spin Fe^{II}–N bond lengths, but are still significantly shorter than those found in high-spin octahedral iron(II) complexes such as $[Fe(thz)_6][Fe_2OCl_4]$ (thz = triazole; 2.21(1) Å)[41] and $[Fe(pyz)_2(NCS)_2]_n$ (pyz = pyrazine; 2.246(2) Å).[42] From the bond length analysis, the iron(II) centre in the $[Fe^{II}(L2)_3]^{2+}$ ion is clearly in the low-spin state.

The counterion in **7**·CH_3CN is the, now well-known,[43] oxo-bridged iron(III) dimer $[Cl_3Fe\text{-}O\text{-}FeCl_3]^{2-}$, formed by the in situ hydrolysis of ferric chloride, first identified by Nelson

and co-workers in 1978.[21, 22, 44] The $[Cl_3Fe^{III}OFe^{III}Cl_3]^{2-}$ ion in **7**·CH_3CN does not possess crystallographically imposed symmetry. The iron(III) atoms, Fe(1) and Fe(2), have approximately tetrahedral geometries, with angles ranging from 109.5(2)° to 111.5(3)° and from 108.7(2)° to 110.8(3)°, respectively. The Fe-O-Fe bond angle, 173.4(4)°, is very close to linear. The $FeCl_3$ moieties are somewhat unevenly bridged by the oxo ion (Fe–O 1.767(6) Å and 1.740(6) Å), but the Fe–O distances are close to the average value observed for this anion (1.76 Å; averaged over 36 crystal structures).[45] The Fe–Cl bonds observed in **7**·CH_3CN (Fe–Cl 2.217(3)–2.240(3) Å) are close to the average observed for the $[Cl_3Fe^{III}OFe^{III}Cl_3]^{2-}$ ion (2.21 Å)[45] and to the values observed for some of the more closely related complexes (also featuring iron(II) ions).[39,40,46] In addition, as was observed by Wieghardt and co-workers,[22] the three Fe–Cl distances within each $FeCl_3$ moiety of the dianion of **7**·CH_3CN are not equivalent: for both iron atoms, one of the three Fe–Cl bonds is somewhat longer than the other two.

Magnetochemistry and Mössbauer spectroscopy: Complexes **1**, **2**, **3**, **4** and **8** are diamagnetic. Variable temperature magnetic susceptibility measurements were made on paramagnetic complexes **5b**, **6b**, **7**·H_2O and **9** in the temperature range 300 to 4 K. Antiferromagnetic exchange between the two metal(II) ions was observed in all of these cases. The results are summarized in Table 2.

Table 2. Magnetic parameters for the paramagnetic dimetallic(II) complexes of L2 obtained using isotropic $-2JS_1S_2$ models.

Complex	S	g	J [cm^{-1}]	ρ[a]	μ_{eff} [μ_B] 295 K, per metal atom
5b	1	2.17	−21.6	0.02	2.89
6b	$^3/_2$	2.44	−7.6	0.02	4.54
9	$^5/_2$	1.95	−3.2	0.02	5.49
7·H_2O	$^5/_2$[b]	1.81	−75[b]	0.025	2.90[c]

[a] Fraction monomer. [b] Value for anion, see text. [c] Per Fe_3.

The magnetic susceptibility data for the Ni^{II} aqua complex **5b** were observed to increase gently from 300 K, reaching a maximum at ~60 K before decreasing rapidly. A sharp increase occurred below 10 K due to monomer impurity (Figure 6). The shape of the plot for χ_M versus T of **5b** shows that there is antiferromagnetic coupling between the two paramagnetic Ni^{II} centres. Of the few structurally characterised doubly pyridazine-bridged-only nickel dimers (see above), those for which an exchange integral (J) is quoted include $[Ni_2(ppd)_2(H_2O)_4]Cl_4 \cdot 2H_2O$, whereby ppd is 3,6-bis(1′-pyrazolyl)pyridazine and $J = -14.8$ cm^{-1},[27] and $[Ni_2(dcpz)_2(H_2O)_4]$, whereby dcpz is 1,4-dicarboxylatopyridazine and $J = -33.6$ cm^{-1}.[29] The J value observed for the doubly pyridazine-bridged dinickel complex **5b**, -21.6 cm^{-1}, falls in this range. The corresponding values of magnetic moment for **5b** decreased with decreasing the temperature reaching 0.48 BM at 4 K. The room temperature magnetic moment of 2.89 BM is indicative of a weakly coupled octahedral nickel(II) ion ($S = 1$) and is comparable to those

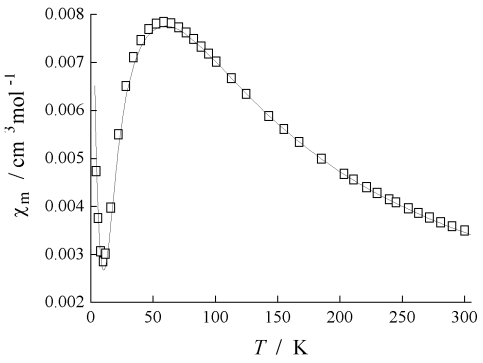

Figure 6. Plot of magnetic susceptibilities, per Ni atom, for complex **5b** versus temperature. The solid line is the best-fit calculated plot using the parameters given in Table 2.

of other binuclear pyridazine-bridged derivatives, for example, $[Ni_2(ppd)_2(H_2O)_4]Cl_4 \cdot 2H_2O$ ($\mu(RT) = 2.95$ μ_B) and $[Ni_2(ppd)_2(H_2O)_4]Br_4$ ($\mu(RT) = 2.99$ μ_B].[27]

The χ_M plots for **6b** show a maximum susceptibility value, at 30 K, and the corresponding μ_{eff} value decreases continuously from room temperature. The behaviour of the complex is typical of high-spin ($S = ^3/_2$) cobalt(II) dimers, which exhibit weak antiferromagnetic exchange between the cobalt(II) centres. A simple $-2JS_1S_2$ Heisenberg model was used to get a good fit. The exchange integral (J) for this high-spin dicobalt(II) complex is -7.6 cm^{-1}, which is slightly lower than those obtained for comparable doubly pyridazine-bridged complexes, for example, $[Co_2L1(H_2O)_4](ClO_4)_4$ in which $J = -9.6$ cm^{-1},[14] and $[Co_2(dcpz)_2(H_2O)_4]$ with $J = -11.5$ cm^{-1}.[29] The binuclear cobalt(II) complex has a room temperature magnetic moment, $\mu(RT) = 4.54$ μ_B, which is lower than values of mononuclear Co^{II}, because of antiferromagnetic coupling. The value is comparable to those observed for related binuclear cobalt(II) complexes, for example, $[Co_2(ppd)_2(H_2O)_4]Cl_4 \cdot 2.5H_2O$ has $\mu_{eff}(RT) = 4.25$ μ_B per cobalt atom, $[Co_2(ppd)_2(H_2O)_4]Br_4$ has $\mu_{eff}(RT) = 4.18$ μ_B per cobalt atom[27] and $[Co_2L1(H_2O)_4](ClO_4)_4$ has $\mu_{eff}(RT) = 3.82$ μ_B.[14]

For the orange dimanganese(II) complex **9**, the value of χ_M gradually increased as the temperature was lowered, to give a maximum in χ_M at very low temperature (Figure 7). Again this behaviour indicates the presence of weak antiferromagnetic interactions between the Mn^{II} ions. At room temperature the

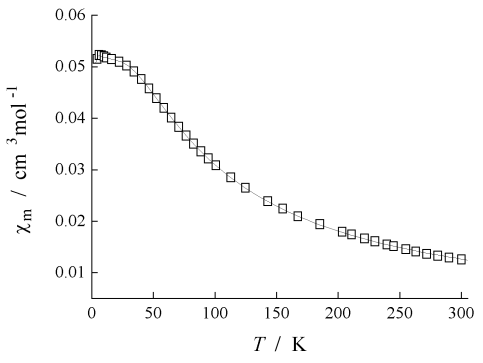

Figure 7. Susceptibility data, per Mn atom, for complex **9**. The solid line is the best-fit calculated plot using the parameters given in Table 2.

μ_{eff} value of **9** is 5.49 μ_B, slightly less than the value of 5.92 μ_B expected for an uncoupled Mn^{2+} ion.[47] It decreased gradually reaching 1.28 μ_B at 4 K. The best fit g value is isotropic at 1.95 and manganese(II) is a well-known example of a Heisenberg ion.[48] A good fit was obtained for a $S = 5/2$ dimer model with $J = -3.2$ cm^{-1}.

The complex **7**·H_2O contains high-spin iron(III) in the anion and low-spin iron(II) in the cation. The Mössbauer spectrum measured at 82 K shows two sharp quadrupole doublets (Figure 8), that for HS Fe^{III} with $\delta = 0.33$ mm s^{-1}, $\Delta E_Q = 1.32$ mm s^{-1} (area 59%) and that for LS Fe^{II} with $\delta = 0.28$ mm s^{-1}, $\Delta E_Q = 0.57$ mm s^{-1} (area 41%). The former doublet is typical of those reported for $[Cl_3FeOFeCl_3]^{2-}$,[21, 49] while the latter is typical of those reported for $[Fe^{II}(N{-}N)_3]^{2+}$ LS chelates.[50]

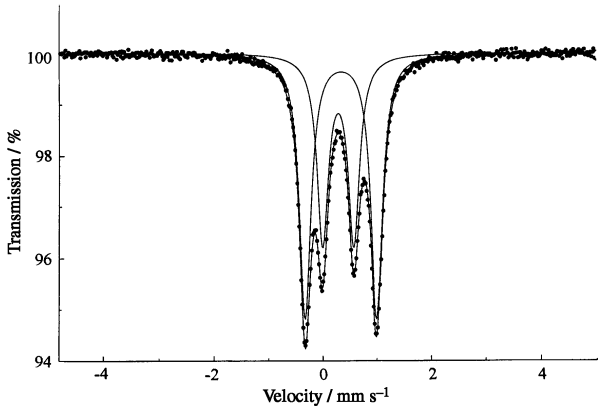

Figure 8. Mössbauer spectrum at 82 K obtained for the double salt iron complex **7**·H_2O.

The magnetic moment at room temperature for the green complex **7**·H_2O is 2.90 μ_B, per Fe_3 unit, and it decreases gradually, in a curved fashion typical of the behaviour of a strongly antiferromagnetically coupled $Fe^{III}OFe^{III}$ compound.[21, 22, 49, 50] The μ_{eff} values reach a plateau of 1.31 μ_B between 60–20 K, then decrease more rapidly to reach 0.90 μ_B at 4 K. The corresponding molar susceptibilities remain largely constant between 300 and 60 K, then increase rapidly down to 4 K. Such behaviour is Curie-like below 60 K indicative of monomer impurity probably combined with a small temperature-independent paramagnetism from the low-spin d^6 cation. A magnetically "pure" $Fe^{III}OFe^{III}$ moiety plus Fe^{II} LS should show no Curie susceptibility tail, but rather a constant decrease in χ between 300 and 4 K, with a small (constant) χ_{TIP} at low temperatures preventing χ reaching zero. The origin of the monomer impurity in **7**·H_2O is not clear, but might, in this case, be an actual trace of chemical impurity rather than, or as well as, the ubiquitous monomer impurities in highly crystalline $[Cl_3FeOFeCl_3]^{2-}$ species.[22, 49] Thus to fit the χ(per Fe_3) data, the Curie values (2.5%), observed below 60 K, were first subtracted at all temperatures, and the remaining $\chi_{(corrected)}$ values fitted to a $S = 5/2$ Heisenberg dimer model. The agreement between observed and calculated χ (or μ) values was quite good, but with some crossing of curves in the range 60–300 K, and the best fit values were $g = 1.81$ and $J = -75$ cm^{-1}. Both of these are lower than normal, g being expected to be close to 2.0 for $^6A_{1g}$ (Fe^{III}) centres, while J values for $[Cl_3FeOFeCl_3]^{2-}$ ions are usually in the range -105 to -117 cm^{-1}.[22] Nevertheless, they do clearly support the presence of this μ-oxo anion combined with the $[Fe^{II}(L2)_3]^{2+}$ ion in the bulk sample, the discrepancies largely emanating from impurities, as described. Interestingly, the Mössbauer spectrum does not reveal any third species such as HS Fe^{II} or HS Fe^{III} and so an HS Fe^{III} contaminant must have very similar parameters to those from $Fe^{III}OFe^{III}$ or have a very weak signal.

Electrochemistry: Cyclic voltammograms of complexes **1**, **2**, **5b**, **6b** and **8** (Figures 9 and 10) have been recorded in 0.001M CH_3CN containing 0.10M $[N(nBu)_4]PF_6$ as supporting electrolyte, at a platinum working electrode and referenced to 0.01M $AgNO_3$/Ag. In all cases the cyclic voltammograms were

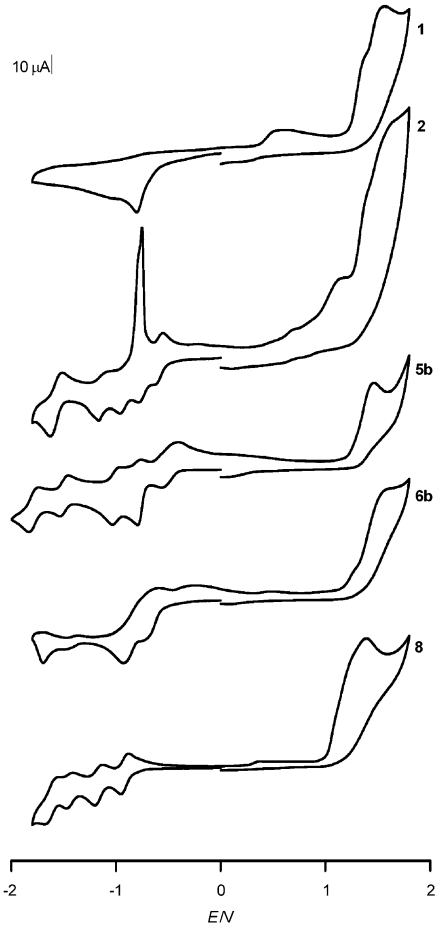

Figure 9. Cyclic voltammograms run at 200 mV s^{-1} in CH_3CN vs. 0.01M $AgNO_3$/Ag. From top to bottom: **1** zinc, **2** copper, **5b** nickel, **6b** cobalt, **8** iron.

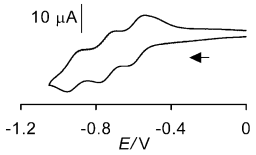

Figure 10. Cyclic voltammogram, run at 200 mV s^{-1} over a narrower potential range than in Figure 9, highlighting the reversible processes for the tetracopper(I) complex **2** in CH_3CN vs. 0.01M $AgNO_3$/Ag.

started at 0.00 V, scanned to the most negative potential and then the scan direction reversed towards the most positive potential before returning to 0.00 V. All potentials quoted in this section were obtained from cyclic voltammograms run at a scan rate of 200 mV s^{-1}. As a reference check, ferrocene was added at the conclusion of each experiment: the Fc^+/Fc couple consistently occurred at $E_{1/2} = +0.07 \pm 0.01$ V with $\Delta E = 0.07$ V in CH_3CN. The reversibility of the redox couples was judged against the usual criteria.[51]

The cyclic voltammogram of the dizinc(II) complex **1**, in the potential range -1.80 to $+1.80$ V, shows one irreversible cathodic process ($E_{pc} = -0.79$ V) and three irreversible anodic processes ($E_{pa} = +0.50$, $+1.37$ and $+1.54$ V) on the reverse scan (Figure 9). The first anodic process ($E_{pa} = +0.50$ V) was not observed if the scan was started from 0.00 V and run to $+1.80$ V before reversing to -1.80 V and back to 0.00 V. Therefore the process is believed to be associated with the cathodic wave at -0.79 V: complex **1** is presumably irreversibly reduced, forming a new compound which can then be oxidised at $+0.50$ V. The Zn^{II} ion is expected to be redox-inert and all observed redox activity can, therefore, be ascribed to ligand-based processes.

The cyclic voltammogram (Figure 9) of the tetracopper(I) complex **2** shows that there are five reduction processes in the potential range of -1.80 to $+1.80$ V. The process at $E_{1/2} = -1.65$ ($\Delta E = 0.13$) V was fully electrochemically reversible, whereas the peak at $E_{pc} = -1.17$ V is not. When the scan direction was reversed at -1.05 V, three reversible anodic waves ($E_{1/2} = -0.93$ ($\Delta E = 0.06$) V, -0.75 ($\Delta E = 0.07$) V and -0.59 ($\Delta E = 0.06$) V) were observed (Figure 10), and the strong anodic stripping peak observed in the full range scan was absent (Figure 9). Controlled potential coulometry at $E_{1/2} = -0.68$, -0.90 and -1.05 V confirmed that each of these three processes corresponds to a one-electron reduction of the initial $[Cu^I_4(L2)_4]^{4+}$ ion. The stripping peak ($E_{pa} = -0.74$ V) is therefore believed to be associated with the fourth reduction process ($E_{pc} = -1.17$ V) generating Cu^0. In addition, two irreversible oxidation processes ($E_{pa} = +1.12$ and $+1.58$ V) were observed. The first oxidation wave is probably due to the oxidation of $Cu^I \rightarrow Cu^{II}$. The second oxidation peak was a very broad, weak, multi-electron process for which the current was slightly increased with increasing scan rate.

These results for **2** are compared, in Table 3, with those reported for the two related pyridazine-based grid systems, $[Cu^I_4(L1)_2]^{4+}$ and $[Cu^I_4(dppn)_4]^{4+}$, although the comparison is complicated by the differing solvent and reference system employed in the case of the dppn compound (DMF, SCE reference).[3a, 13] In all three cases three reversible one-electron processes are observed at negative potentials, but the $E_{1/2}$ values for these processes vary somewhat from complex to complex. In addition, a fourth reversible one-electron process was obtained in the cyclic voltammograms of $[Cu^I_4(L1)_2]^{4+}$ and $[Cu^I_4(dppn)_4]^{4+}$. However, in the case of acyclic **2** a strong stripping anodic wave was observed instead of a reversible process when the fourth reduction was attempted. No stripping peak is observed for the macrocyclic complex, even when the scan direction is not reversed until -2.00 V, consistent with the common observation that macrocyclic ligands stabilize redox products to a greater extent than acyclic ligands can. It is interesting to note that acyclic **2** is more easily reduced than the closely related macrocyclic analogue $[Cu^I_4(L1)_2]^{4+}$, presumably due to the greater degree of conjugation present in L2 over that in L1. In the case of $[Cu^I_4(L1)_2]^{4+}$ and $[Cu^I_4(dppn)_4]^{4+}$ the four processes are believed to be predominately ligand-centred, whereas in **2** the fourth reduction process is thought to be metal-centred, $Cu^I \rightarrow Cu^0$, generating the stripping peak on the return scan (see above).

Table 3. Comparison of electrochemical data, obtained from cyclic voltammograms, for $[Cu^I_4(L2)_4]^{4+}$, $[Cu^I_4(L1)_2]^{4+}$ and $[Cu^I_4(dppn)_4]^{4+}$.

Complex	$E^4_{1/2}$	$E^3_{1/2}$	$E^2_{1/2}$	$E^1_{1/2}$	Ref.
$[Cu^I_4(L2)_4]^{4+}$	-1.17[a,c]	-0.93[a]	-0.75[a]	-0.59[a]	this work
$[Cu^I_4(L1)_2]^{4+}$	-1.35[a]	-1.13[a]	-0.87[a]	-0.69[a]	[13]
$[Cu^I_4(dppn)_4]^{4+}$	-1.32[b]	-1.16[b]	-1.01[b]	-0.88[b]	[3a]

[a] CH_3CN vs. 0.01M $AgNO_3$/Ag. [b] DMF vs SCE. [c] Value given is E_{pc}, not $E_{1/2}$.

Cyclic voltammetry studies on the dinickel(II) complex **5b** reveal that this species also has many redox processes (Figure 9). There are two fully reversible reduction processes ($E_{1/2} = -1.79$ V ($\Delta E = 0.07$ V), -1.50 V ($\Delta E = 0.06$ V)) and a quasi-reversible process ($E_{1/2} = -0.48$ V ($\Delta E = 0.13$ V)). In addition, three irreversible processes were observed at $E_{1/2} = -1.01$ V ($\Delta E = 0.05$ V), -0.78 V ($\Delta E = 0.02$ V) and $E_{pa} = +1.45$ V. Scan rate studies were carried out on the former two irreversible processes. The current of the cathodic processes went up with the increase of scan rate, but the current of the associated anodic processes almost dropped down to zero. These redox processes are again believed to be predominately ligand-centred.

The cyclic voltammogram of dicobalt(II) complex **6b** (Figure 9) displays one fully reversible redox process ($E_{1/2} = -1.45$ V ($\Delta E = 0.08$ V)), a quasi-reversible process [$E_{1/2} = -0.96$ V ($\Delta E = 0.20$ V)] and four irreversible processes ($E_{pc} = -1.72$, -0.72 V and $E_{pa} = +1.23$, $+1.55$ V). The first reduction process ($E_{1/2} = -1.45$ V) was very weak at the 200 mV s^{-1} scan rate (Figure 9), but it is reversible; the current proportionally increased with increasing $\nu^{1/2}$ and the process also met all of the other requirements for reversibility.[51] If the scan was reversed at -0.80 V, no anodic waves were observed so the process at $E_{pc} = -0.72$ V is totally irreversible. However, an anodic peak is obtained if the scan was reversed at -1.30 V and the process at $E_{1/2} = -0.96$ V is therefore electrochemically quasi-reversible. A very weak anodic wave was observed at $+1.23$ V, which may be due to the oxidation of $Co^{II} \rightarrow Co^{III}$. The only pyridazine-bridged cobalt complex for which cyclic voltammetric data have been reported is $[Co^{II}(L1)(CH_3CN)_4]^{4+}$.[10] In that case, four reversible waves were observed at much more accessible potentials -0.33, -0.11, $+0.87$ and $+1.06$ V versus 0.01M $AgNO_3$/Ag. These processes were tentatively interpreted as being predominately metal-centred, but the distinct possibility that the L1 ligand is non-innocent must be examined.[52]

The cyclic voltammogram of mono-iron(II) complex **8** shows that it is redox active (Figure 9). There are three successive fully reversible processes ($E_{1/2} = -1.44$ V ($\Delta E = 0.06$ V), -1.17 V ($\Delta E = 0.06$ V) and -0.91 V ($\Delta E = 0.07$ V)) followed by a quasi-reversible process ($E_{1/2} = -1.62$ V ($\Delta E = 0.09$ V)).

Coulometry at $E_{1/2} = -1.50$ V established that the $[Fe^{II}(L2)_3]^{2+}$ ion undergoes three successive one-electron reductions. A very weak quasi-reversible oxidation process ($E_{1/2} = +0.28$ V ($\Delta E = 0.13$ V)) could be observed on the reverse scan at this scan rate. In addition, a multiple electron oxidation process is observed at +1.37 V.

Conclusion

Control of molecular architecture by metal-ion coordination geometry preferences has been illustrated by the formation of two very different structural types from the same Schiff base ligand, L2. This demonstration that Schiff bases are good ligands for the formation of such grid and array type complexes means that the nature and properties of such supramolecular arrays can be easily varied and tuned. As such these complexes, which include examples of complexes of all of the first row transition metal ions from Zn^{II} to Mn^{II}, are important illustrations of the use of coordination algorithms and are likely to be the first of many.

The observation of a third outcome (cf. Scheme 1), due to iron(II) preferring to go low spin by binding three L2 ligands, even when the ratio of metal:ligand was only 1:1, was disappointing. It had been hoped that a side-by-side architecture (similar to that observed for **1**, **5a** and **6a**) would be observed for this octahedral metal ion, and that the ligand field might be in the range to generate a spin-crossover complex by choice of appropriate axial ligands.[14] Our efforts are now directed towards varying the amines condensed with 3,6-diformylpyridazine to tune the properties of the complexes and/or generate bigger arrays, and also the use of other heterocycles in the generation of grid-type architectures of octahedral metal ions with the intention of generating species with reversible metal-based redox processes and/or spin-crossover behaviour.[16]

Experimental Section

3,6-Diformylpyridazine was synthesised according to the literature preparation.[5, 7] *p*-Anisidine was recrystallised from aqueous ethanol after decolourising with activated carbon. $[Cu(CH_3CN)_4]BF_4$ was prepared according to the procedure outlined by Kubas.[53] Where noted, acetonitrile was refluxed over calcium hydride and distilled prior to use, otherwise HPLC grade acetonitrile was used as received.

Caution!: *Whilst no problems were encountered in the course of this work perchlorate mixtures are potentially explosive and should therefore be handled with appropriate care.*

X-ray data were collected on a Bruker SMART diffractometer ($\lambda =$ 0.71073 Å) and the structures solved and refined by using SHELXS and SHELXL.[54–56] CCDC-204611–204615 contain the supplementary crystallographic data for this paper. These data can be obtained free of charge via www.ccdc.cam.ac.uk/conts/retrieving.html (or from the Cambridge Crystallographic Data Centre, 12 Union Road, Cambridge CB2 1EZ, UK; fax: (+44) 1223-336033; or deposit@ccdc.cam.ac.uk). The magnetic susceptibilities were measured by using a Quantum Design MPMS 5 Squid magnetometer as described previously.[13, 14] The Mössbauer spectrum was obtained using a conventional constant acceleration drive with a symmetrical sawtooth waveform. The source of ^{57}Co in rhodium was maintained at room temperature. The iron complex was loaded into a piston type Perspex holder. The holder was placed in a cold-finger type cryostat in good thermal contact with the reservoir that contained liquid nitrogen. Drive calibration was carried out using an α-Fe foil and isomer shifts are quoted relative to α-Fe at room temperature. The spectrum was fitted to Lorentzian lines, with the matching lines of a doublet constrained to have the same intensity and linewidth. All other measurements were carried out as described previously.[7, 13]

Ligand L2: A colourless solution of *p*-anisidine (1.2570 g, 10.2 mmol) in ethanol solution (20 cm^3) was added to a stirred yellow solution of 3,6-diformylpyridazine (0.6950 g, 5.1 mmol) in reagent grade ethanol (20 cm^3). The initially clear, pale lemon solution became increasingly opaque as a fine precipitate started to form within minutes of the addition. The reaction mixture was stirred for 4 h at room temperature before the fine lemon yellow powder, L2 ($H_3COPhN{=}CHC_4H_2N_2CH{=}NPhOCH_3$), was filtered off, washed with ethanol (5 cm^3) and dried in vacuo (1.6421 g, 93%). Elemental analysis calcd (%) for $C_{20}H_{18}N_4O_2$: C 69.35, H 5.24, N 16.17; found: C 69.14, H 5.29, N 16.04; IR (KBr disk, inter alia): $\tilde{\nu} = 3475$ (br w), 1622 (s), 1593 (s), 1577 (s), 1503 (vs), 1464 (m), 1290 (s), 1243 (vs), 1163 (s), 1031 (s), 967 (m), 830 (s), 755 (m), 561 cm^{-1} (m); ^{1}H NMR (500 MHz, solvent $CDCl_3$, reference $CHCl_3$@7.26 ppm): $\delta = 8.99$ (s, 2H; H6), 8.43 (s, 2H; H3), 7.42 (d, $^3J_{9,10} = 9.0$ Hz, 4H; H9), 6.99 (d, $^3J_{9,10} = 9.0$ Hz, 4H; H10), 3.86 ppm (s, 6H; H14); ^{13}C NMR (125 MHz, solvent $CDCl_3$, reference $CHCl_3$@77.3 ppm): $\delta = 159.8$ (C11), 158.1 (C2), 154.9 (C6), 143.0 (C8), 124.7 (C3), 123.2 (C9), 114.7 (C10), 55.6 ppm (C14); UV/Vis (DMF): λ_{max} (ε) = 292 (15800), 384 nm (35000 dm^{3}mol^{-1}cm^{-1}); Mass spectrum (EI): *m*/*z*: 346 [M^+], 345 [$M^+ - H$], 331 [$M^+ - CH_3$], 315 [$M^+ - OCH_3$].

$[Zn^{II}_2(L2)_2(H_2O)_2(CH_3CN)_2][ClO_4]_4$ (1): A colourless solution of $Zn(ClO_4)_2 \cdot 6H_2O$ (0.0372 g, 0.10 mmol) in acetonitrile (5 cm^3) was added dropwise to a stirred lemon yellow suspension of L2 (0.0346 g, 0.10 mmol) in acetonitrile (15 cm^3), causing an immediate colour change to orange. The resulting orange solution was stirred at room temperature for 6 h, after which time it was reduced in volume (ca. 6 cm^3). **1**·CH_3CN was isolated as orange needle-like crystals by fast vapour diffusion of diethyl ether vapour into the reaction solution, and, on drying in vacuo, gave **1** (0.0589 g, 96%). Elemental analysis calcd (%) for $C_{40}H_{36}N_8Zn_2Cl_4O_{20}$ (**1**) without the coordinated solovent: C 39.34, H 2.97, N 9.17; found: C 39.29, H 3.37, N 9.29; IR (KBr disk, inter alia): $\tilde{\nu} = 3447$ (br s), 1622 (w), 1599 (m), 1508 (m), 1304 (w), 1258 (m), 1168 (m), 1121 (s), 1030 (m), 827 (m), 625 cm^{-1} (m); ^{1}H NMR (500 MHz, solvent CD_3CN, reference CH_3CN@1.94 ppm): $\delta =$ 8.87 (br s, 2H; H6), 8.57 (br s, 2H; H3), 7.45 (br m, 4H; H9), 7.07 (br m, 4H; H10), 3.85 ppm (s, 6H; H14); ^{13}C NMR (125 MHz, solvent CD_3CN, reference CH_3CN@1.32 ppm): $\delta = 161.8$, 161.7 (C11, C2), 125.1 (C6), 125.0 (C8), 116.0 (C3), 115.9 (C9), 115.8 (C10), 56.4 ppm (C14); UV/Vis (CH_3CN): λ_{max} (ε) = 245 (36000), 396 nm (46500 dm^{3}mol^{-1}cm^{-1}); Λ_m (CH_3CN) = 450 mol^{-1}cm$^2\,\Omega^{-1}$ (cf. 340 to 420 for a 3:1 electrolyte in CH_3CN);[23] MS (ES): *m*/*z*: 768 $[Zn_2L2(CH_3CN)_3(H_2O)_4(ClO_4)]^+$, 750 $[Zn_2L2(CH_3CN)_3(H_2O)_3(ClO_4)]^+$, 668 $[ZnL2(CH_3CN)_3(H_2O)_2(ClO_4)]^+$, 650 $[ZnL2(CH_3CN)_3(H_2O)(ClO_4)]^+$, 551 $[ZnL2(CH_3CN)_3(H_2O)]^+$, 492 $[ZnL2(CH_3CN)_2]^+$, 347 $[L2 + H]^+$.

$[Cu^I_4(L2)_4](PF_6)_4$ (2): Ligand L2 (0.174 g, 0.504 mmol) was suspended in freshly distilled acetonitrile (20 cm^3) and degassed by argon for 15 min. $[Cu^I_4(CH_3CN)_4]PF_6$ (0.188 g, 0.503 mmol) was added as a solid to this stirred lemon yellow suspension under an argon atmosphere. Immediately the mixture turned dark brown. After 10 min of stirring, the L2 ligand had completely dissolved to form a clear dark brown solution. The mixture was allowed to stir at room temperature for 2 h. Dark brown needle-like crystals of **2**·$(CH_3CN)(H_2O)(CH_3CH_2OCH_2CH_3)_{0.25}$ were obtained by diethyl ether vapour diffusion into the reaction solution in air. The crystals were isolated and dried in vacuo to yield **2** (0.250 g, 89%). Elemental analysis calcd (%) for $C_{80}H_{72}N_{16}Cu_4P_4F_{24}O_8$ (**2**): C 43.3, H 3.3, N 10.1; found: C 43.3, H 3.4, N 10.0; IR (KBr disk, inter alia): $\tilde{\nu} = 3446$ (m), 1613 (m), 1575 (s), 1505 (s), 1406 (m), 1306 (m), 1293 (m), 1265 (s), 1250 (s), 1165 (s), 1070 (w), 1024 (w), 835 (vs), 557 cm^{-1} (m); ^{1}H NMR (300 MHz, solvent CD_3NO_2, reference CH_3NO_2@4.33 ppm): $\delta = 9.24$ (s, 2H; H6), 8.60 (s, 2H; H3), 7.16 (d, $^3J_{9,10} = 9.13$ Hz, 4H; H9), 6.50 (d, $^3J_{9,10} = 9.13$ Hz, 4H; H10), 3.67 ppm (s, 6H; H14); ^{13}C NMR (125 MHz, solvent CD_3NO_2, reference CH_3NO_2@62.8 ppm): $\delta = 163.9$ (C11), 156.5 (C2), 150.4 (C6), 138.6 (C8), 134.2 (C3), 126.5 (C9), 116.4 (C10), 56.4 ppm (C14); UV/Vis (CH_3CN): λ_{max} (ε) = 236 (sh), 290 (66700), 378 nm (143300 dm^{3}mol^{-1}cm^{-1}); Λ_m (CH_3CN) = 412 mol^{-1}cm$^2\,\Omega^{-1}$ (cf. 340 to 420 for a 3:1 electrolyte in CH_3CN);[23] MS (FAB): *m*/*z*: 1928 $[Cu_4(L2)_4(PF_6)_2]^+$, 1783

$[Cu_4(L2)_4(PF_6)]^+$, 963 $[Cu_2(L2)_2PF_6]^+$, 820 $[Cu_2(L2)_2]^+$, 755 $[Cu(L2)_2]^+$, 409 $[Cu(L2)]^+$.

$[Cu^I_2(L2)_2(NCS)_2]\cdot H_2O$ (3): Ligand L2 (0.0346 g, 0.10 mmol) was suspended in freshly distilled acetonitrile (20 cm^3) and degassed by nitrogen for 15 min. $[Cu(CH_3CN)_4](BF_4)$ (0.0315 g, 0.10 mmol) was added as a solid to the stirred yellow suspension under a nitrogen atmosphere, causing an immediate colour change to intense brown. Over 20 min, ligand L2 dissolved completely to form an intense brown solution. NaSCN (0.0098 g, 0.12 mmol) as a solid was added to the stirred solution, with no apparent change. The solution was stirred for 4 h during which time a greenish brown precipitate formed. The intense greenish brown powder was filtered off, washed with acetonitrile (5 cm^3), and dried in vacuo to give **3** (0.0417 g, 87%). Elemental analysis calcd (%) for $C_{42}H_{36}N_{10}Cu_2O_4S_2\cdot H_2O$ (**3**): C 52.88, H 4.01, N 14.68, S 6.72; found: C 52.85, H 3.71, N 15.01, S 7.00; IR (KBr disk, inter alia): $\tilde{\nu}=3480$ (br w), 2112 (s), 1619 (w), 1587 (m), 1503 (s), 1463 (w), 1291 (m), 1245 (s), 1163 (m), 1027 (m), 835 cm^{-1} (m); ^1H NMR (500 MHz, solvent DMF, reference DMF@2.74 ppm): $\delta=9.10$ (s, 2H; H6), 8.53 (s, 2H; H3), 7.60 (d, $^3J_{9,10}=8.58$ Hz, 4H; H9), 7.10 (d, $^3J_{9,10}=8.28$ Hz, 4H; H10), 3.88 ppm (s, 6H; H14); ^{13}C NMR (125 MHz, solvent DMF, reference DMF@30.1 ppm): $\delta=124.3$ (C9), 115.3 (C10), 55.9 ppm (C14); UV/Vis (DMF): λ_{max} (ε) = 292 (27800), 383 nm (61100 $dm^3mol^{-1}cm^{-1}$). Λ_m (DMF) = 15 $mol^{-1}cm^2\Omega^{-1}$ (cf. 65 to 90 for a 1:1 electrolyte in DMF).[23] MS (ES): *m/z*: 563 $[Cu(L2)(NCS)_2(H_2O)_2]^+$, 545 $[Cu(L2)(NCS)_2(H_2O)]^+$, 463 $[Cu(L2)(NCS)]^+$, 347 $[L2+H]^+$, 124 $[Cu(NCS)]^+$.

$[Cu^I_2(L2)(NCS)_2]$ (4): Ligand L2 (0.0346 g, 0.10 mmol) was suspended in freshly distilled acetonitrile (20 cm^3) and degassed by nitrogen for 15 min. $[Cu(CH_3CN)_4](BF_4)$ (0.0629 g, 0.20 mmol) was added as a solid to the stirred yellow suspension under a nitrogen atmosphere, causing an immediate colour change to intense brown. After 20 min NaSCN (0.0162 g, 0.20 mmol) was added as a solid, with no apparent colour change. The mixture was stirred for 4 h during which time an intense brown (almost black by eye) precipitate formed. The powdery precipitate was filtered off, washed with acetonitrile (5 cm^3) and dried in vacuo to give **4** (0.0536 g, 91%). Elemental analysis calcd (%) for $C_{22}H_{18}N_6Cu_2O_2S_2$ (**4**): C 44.81, H 3.08, N 14.25, S 10.87; found: C 44.51, H 2.96, N 14.25, S 10.82; IR (KBr disk, inter alia): $\tilde{\nu}=3463$ (br w), 2111 (s), 1616 (w), 1586 (m), 1503 (s), 1290 (m), 1245 (s), 1163 (s), 1026 (m), 841 cm^{-1} (m).

$[Ni^{II}_2(L2)_2X_4][BF_4]_4$ (X = CH_3CN 5a; X = H_2O 5b): A pale blue solution of $Ni(BF_4)_2\cdot 6H_2O$ (0.0340 g, 0.10 mmol) in acetonitrile (5 cm^3) was added dropwise to a lemon yellow suspension of L2 (0.0346 g, 0.10 mmol) in acetonitrile (15 cm^3), causing an immediate colour change to brown-red. The resulting brownish red solution was stirred at room temperature for 4 h after which time the solution was reduced in volume (ca. 10 cm^3). Dark red single crystals of **5a**$\cdot(CH_3CH_2OCH_2CH_3)_{0.25}$ formed by slow vapour diffusion of diethyl diethyl ether vapour into the reaction solution. These were filtered off, washed with acetonitrile (5 cm^3) and dried in vacuo to give **5b** (0.0480 g, 78%). Elemental analysis calcd (%) for $C_{40}H_{36}N_8Ni_2B_4F_{16}O_4\cdot 4H_2O$ (**5b**): C 39.08, H 3.61, N 9.11; found: C 39.09, H 3.72, N 9.11; IR (KBr disk, inter alia): $\tilde{\nu}=3420$ (br m), 1619 (w), 1599 (s), 1507 (s), 1304 (m), 1259 (s), 1169 (s), 1083 (s), 1032 (m), 828 (w), 533 (w), 521 cm^{-1} (w); UV/Vis (CH_3CN): λ_{max} (ε) = 250 (sh), 412 (39200), 866 nm (57 $dm^3mol^{-1}cm^{-1}$); Λ_m (CH_3CN) = 398 $mol^{-1}cm^2\Omega^{-1}$ (cf. 340 to 420 for a 3:1 electrolyte in CH_3CN);[23] MS (ES): *m/z*: 769 $[Ni(L2)(H_2O)(BF_4)_4]^+$, 549 $[Ni(L2)(H_2O)(CH_3CN)(BF_4)]^+$; magnetic moment $\mu_{eff}=2.89$ μ_B per Ni at 298 K.

$[Co^{II}_2(L2)_2Y_2](ClO_4)_4$ (X = CH_3CN, Y = H_2O 6a; X = Y = H_2O 6b): $Co(ClO_4)_2\cdot 6H_2O$ (0.107 g, 0.292 mmol) was added as a solid to a stirred lemon yellow suspension of L2 (0.102 g, 0.294 mmol) in acetonitrile (30 cm^3). Immediately the mixture turned dark red. After 20 min of stirring, the ligand L2 had completely dissolved to form a clear dark red solution. The resulting intense red solution was allowed to stir at room temperature for 2 h, after which time the solution was reduced to half of the original volume. Dark red crystals of **6a**$\cdot(H_2O)(CH_3CN)_{0.5}$ were obtained by diethyl ether vapour diffusion into the reaction solution. The crystals were isolated and dried in vacuo to yield **6b** (0.165 g, 88%). Elemental analysis calcd (%) for $C_{40}H_{36}N_8Co_2Cl_4O_{20}\cdot 4H_2O$ (**6b**): C 37.52, H 3.46, N 8.75; found: C 37.42, H 3.56, N 8.72; IR (KBr disk, inter alia): $\tilde{\nu}=3415$ (m), 1617 (m), 1598 (s), 1506 (s), 1442 (w), 1303 (m), 1259 (m), 1169 (s), 1145 (s), 1115 (s), 1080 (s), 1028 (m), 924 (w), 833 (w), 625 cm^{-1} (m); UV/Vis (CH_3CN): λ_{max} (ε) = 244 nm (sh), 406 (50100), 921 nm (29 $dm^3mol^{-1}cm^{-1}$); Λ_m (CH_3CN) = 411 $mol^{-1}cm^2\Omega^{-1}$ (cf. 340 to 420 for a 3:1 electrolyte in CH_3CN);[23] MS (FAB): *m/z*: 850 $[Co(L2)_2(ClO_4)]^+$, 751 $[Co(L2)_2]^+$, 405 $[Co(L2)]^+$; magnetic moment $\mu_{eff}=4.54$ μ_B per Co at 298 K. The cobalt(II) complex showed no oxidation instability in acetonitrile solution, so no precaution was taken to exclude air during the preparation of complex **6**.

$[Fe^{II}(L2)_3][Fe^{III}Cl_3OCl_3Fe^{III}]$ (7): Ligand L2 (0.1039 g, 0.30 mmol) was suspended in freshly distilled acetonitrile (50 cm^3) and degassed by nitrogen for 15 min. Solid $FeCl_2\cdot 4H_2O$ (0.0597 g, 0.30 mmol) was added to this lemon yellow suspension under a nitrogen atmosphere. Immediately the mixture turned dark green. The resulting mixture was stirred at room temperature for 4 h during which time an intense green powder precipitated. Green crystals of **7**$\cdot CH_3CN$ were obtained by diethyl ether vapour diffusion into an acetonitrile reaction filtrate. The resulting green precipitate was filtered off, washed with dry acetonitrile (5 cm^3) and dried in vacuo to yield **7**$\cdot H_2O$ (0.1113 g, 77%). Elemental analysis calcd (%) for $C_{60}H_{54}N_{12}Fe_3Cl_6O_7\cdot H_2O$ (**7**$\cdot$**H**$_2$**O**): C 49.58, H 3.88, N 11.56, Cl 14.64; found: C 49.83, H 3.71, N 11.68, Cl 14.61; IR (KBr disk, inter alia): $\tilde{\nu}=3417$ (br w), 1604 (m), 1570 (m), 1502 (s), 1300 (w), 1253 (s), 1163 (s), 1026 (m), 833 cm^{-1} (m); UV/Vis (CH_3NO_2): λ_{max} (ε) = 419 (66700), 599 nm (10800 $dm^3mol^{-1}cm^{-1}$); Λ_m (CH_3NO_2) = 30 $mol^{-1}cm^2\Omega^{-1}$ (cf. 75 to 95 for a 1:1 electrolyte in CH_3NO_2);[23] MS in CH_3NO_2 (ES): *m/z*: 547 $[Fe(L2)_3]^{2+}$; magnetic moment $\mu_{eff}=2.90$ μ_B per Fe_3 at 298 K.

$[Fe^{II}(L2)_3](BF_4)_2\cdot 2H_2O$ (8): Ligand L2 (0.1038 g, 0.30 mmol) was suspended in freshly distilled acetonitrile (30 cm^3) and degassed by nitrogen for 15 min. Solid $Fe(BF_4)_2\cdot 6H_2O$ (0.0338 g, 0.10 mmol) was added to this yellow suspension under a nitrogen atmosphere, causing an immediate colour change to dark brown. Over about 1 min, the dark brown mixture turned intense green. The mixture was stirred at room temperature overnight. A small amount of yellow precipitate was filtered off, washed with acetonitrile (5 cm^3) and dried in vacuo (0.4 mg). Infrared spectroscopy showed that the precipitate was recovered ligand L2. The filtrate was reduced in volume (ca. 10 cm^3) and the vapour diffusion of diethyl ether vapour into this solution gave **8** as a dark green crystalline solid, which was filtered off and dried in vacuo (0.1028 g, 79%); Elemental analysis calcd (%) for $C_{60}H_{54}N_{12}O_6FeB_2F_8\cdot 2H_2O$ (**8**): C 55.24, H 4.48, N 12.88; found: C 55.51, H 4.28, N 13.03; IR (KBr disk, inter alia): $\tilde{\nu}=3413$ (br w), 1604 (m), 1571 (m), 1503 (s), 1463 (w), 1295 (m), 1249 (s), 1163 (s), 1083 (s), 1026 (s), 835 (m), 533 (w), 521 cm^{-1} (w); ^1H NMR (500 MHz, solvent CD_3CN, reference CH_3CN@1.94 ppm): $\delta=9.10$, 9.03, 8.93, 8.83, 8.69, 8.46 (s, 6H; H6); 8.63, 8.56, 8.47, 8.40, 8.21, 8.13 (d, 6H; H3); 7.62, 7.43, 7.40, 7.11, 7.01, 6.97 (d, 6H; H9); 6.96, 6.89, 6.85, 6.67, 6.56, 6.29 (d, 6H; H10); 3.88, 3.82, 3.79, 3.73, 3.72, 3.65 ppm (s, 6H; H14); ^{13}C NMR (125 MHz, solvent CD_3CN, reference CH_3CN@1.32 ppm): $\delta=170.42$, 170.16, 167.85, 167.57, 166.96, 166.68, 163.63, 163.00, 162.88, 161.68, 161.53, 161.49, 161.30, 161.21, 160.58, 160.52, 160.22, 153.93, 153.79, 153.64, 153.16, 152.90, 145.74, 142.95, 141.91, 141.06, 133.20, 132.97, 125.98, 125.26, 125.16, 124.95, 124.84, 124.71, 124.60, 124.39, 115.76, 115.59, 115.53, 115.36, 115.27, 115.16, 56.50, 56.42, 56.31, 56.28, 56.25, 56.19 ppm; UV/Vis (CH_3CN): λ_{max} (ε) = 416 (80100), 599 nm (12200 $dm^3mol^{-1}cm^{-1}$); Λ_m (CH_3CN) = 273 $mol^{-1}cm^2\Omega^{-1}$ (cf. 220 to 300 for a 2:1 electrolyte in CH_3CN);[23] MS (ES): *m/z*: 547 $[Fe(L2)_3]^{2+}$, 785 $[Fe(L2)_2(H_2O)_2]^+$, 767 $[Fe(L2)_2(H_2O)]^+$; magnetic moment $\mu_{eff}=0$ μ_B per Fe at 298 K.

$[Mn^{II}_2(L2)_2Cl_4]\cdot 3H_2O$ (9): $MnCl_2\cdot 4H_2O$ (0.0198 g, 0.10 mmol) was added as a pink solid to a stirred lemon yellow suspension of L2 (0.0346 g, 0.10 mmol) in acetonitrile (20 cm^3). The resulting orange-yellow mixture was stirred at room temperature for 6 h, during which time **9** precipitated as an orange powder. The precipitate was filtered off and dried in vacuo (0.0388 g, 78%). Elemental analysis calcd (%) for $C_{40}H_{36}N_8Mn_2Cl_4O_4\cdot 3H_2O$ (**9**): C 48.12, H 4.24, N 11.22, Cl 14.20; found: C 48.28, H 3.90, N 11.36, Cl 14.51; IR (KBr disk, inter alia): $\tilde{\nu}=3445$ (br m), 1623 (m), 1588 (w), 1505 (s), 1442 (w), 1300 (m), 1246 (s), 1164 (m), 1107 (w), 1028 (m), 833 cm^{-1} (m); UV/Vis (DMF): λ_{max} (ε) = 293 (23600), 383 nm (60300 $dm^3mol^{-1}cm^{-1}$); Λ_m(DMF) = 50 $mol^{-1}cm^2\Omega^{-1}$ (cf. 65 to 90 for a 1:1 electrolyte in DMF);[23] MS in DMF (ES): *m/z*: 907 $[Mn_2(L2)_2Cl_3]^+$, 782 $[Mn(L2)_2Cl]^+$, 546 $[Mn(L2)Cl_2(DMF)]^+$, 509 $[Mn(L2)Cl(DMF)]^+$, 435 $[Mn(L2)Cl]^+$, 347 $[L2+H]^+$; magnetic moment $\mu_{eff}=5.49$ μ_B per Mn at 298 K.

Crystal data for 1$\cdot CH_3CN$: Orange, $T=168$ K, $C_{46}H_{49}Cl_4N_{11}O_{22}Zn_2$, $M_r=1380.50$, monoclinic, *C*2/*c*, $a=12.560(10)$, $b=26.04(2)$, $c=17.388(13)$ Å, $\beta=98.629(15)^\circ$, $V=5623(8)$ Å^3, $Z=4$, $\mu=1.13$ mm^{-1}, 36013 reflections collected. $R1=0.0526$ [for 1706 $F>4\sigma(F)$; $wR2=0.2026$ and goodness of fit = 0.710 for all 5631 independent F^2; 416 parameters].

Crystal data for $2\cdot(CH_3CN)(H_2O)(CH_3CH_2OCH_2CH_3)_{0.25}$: Red-black, $T=163$ K, $C_{83}H_{79.5}Cu_4F_{24}N_{17}O_{9.25}P_4$, $M_r=2297.18$, triclinic, $P\bar{1}$, $a=13.565(5)$, $b=15.191(5)$, $c=27.295(9)$ Å, $\alpha=77.952(4)^\circ$, $\beta=88.800(4)^\circ$, $\gamma=80.560(4)^\circ$, $V=5426(3)$ Å^3, $Z=2$, $\mu=0.93$ mm^{-1}, 51609 reflections collected. $R1=0.0804$ [for 12028 $F>4\sigma(F)$; $wR2=0.2991$ and goodness of fit = 1.071 for all 20517 independent F^2; 1346 parameters].

Crystal data for $5a\cdot(CH_3CH_2OCH_2CH_3)_{0.25}$: Red, $T=168$ K, $C_{49}H_{50.5}B_4F_{16}N_{12}Ni_2O_{4.25}$, $M_r=1340.17$, monoclinic, $P2_1/n$, $a=16.267(6)$, $b=20.109(7)$, $c=18.546(7)$ Å, $\beta=96.008(6)^\circ$, $V=6034(4)$ Å^3, $Z=4$, $\mu=0.727$ mm^{-1}, 76301 reflections collected. $R1=0.0912$ [for 7000 $F>4\sigma(F)$; $wR2=0.1659$ and goodness of fit = 1.042 for all 12130 independent F^2; 818 parameters].

Crystal data for $6a\cdot(H_2O)(CH_3CN)_{0.5}$: Red, $T=163$ K, $C_{45}H_{49.5}Cl_4Co_2N_{10.5}O_{23}$, $M_r=1365.11$, triclinic, $P\bar{1}$, $a=10.590(3)$, $b=18.060(6)$, $c=18.568(6)$ Å, $\alpha=64.907(4)^\circ$, $\beta=85.981(4)^\circ$, $\gamma=76.493(4)^\circ$, $V=3125.6(17)$ Å^3, $Z=2$, $\mu=0.783$ mm^{-1}, 39480 reflections collected. $R1=0.0774$ [for 8896 $F>4\sigma(F)$; $wR2=0.2730$ and goodness of fit = 1.075 for all 12504 independent F^2; 838 parameters].

Crystal data for $7\cdot CH_3CN$: Green, $T=163$ K, $C_{62}H_{57}Cl_{16}Fe_3N_{13}O_7$, $M_r=1476.46$, triclinic, $P\bar{1}$, $a=13.072(13)$, $b=14.483(14)$, $c=20.094(18)$ Å, $\alpha=74.231(16)^\circ$, $\beta=82.912(14)^\circ$, $\gamma=66.200(13)^\circ$, $V=3349(5)$ Å^3, $Z=2$, $\mu=0.942$ mm^{-1}, 43681 reflections collected. $R1=0.0587$ [for 1512 $F>4\sigma(F)$; $wR2=0.1094$ and goodness of fit = 0.691 for all 13402 independent F^2; 532 parameters].

Acknowledgement

This work was supported by grants from the University of Otago, Athabasca University and the Australian Research Council (ARC Discovery). We are grateful to the University of Otago for awarding Y.L. an Otago Postgraduate Scholarship, Athabasca University for granting D.K.K. study leave and Professor W. T. Robinson and Dr. J. Wikaira (University of Canterbury) for the X-ray data collections. S.B. thanks the University of Otago for the granting of study leave which allowed the completion of some of these structural analyses and the initial draft of this manuscript to be prepared, and gratefully acknowledges her hosts Professors M. D. Ward and J. McCleverty and Dr. J. C. Jeffery (Bristol University), and the financial support of a Royal Society of Chemistry Journals Grant. The front cover image was kindly generated by M. Crawford (University of Otago) with Strata Studio Pro (Strata).

[1] J.-M. Lehn, *Chem. Eur. J.* **2000**, *6*, 2097.
[2] See for example: a) S. Leininger, B. Olenyuk, P. J. Stang, *Chem. Rev.* **2000**, *100*, 853–908; b) R. Robson, *J. Chem. Soc. Dalton Trans.* **2000**, 3735–3744; c) N.-D. Sung, K.-S. Yun, T.-Y. Kim, K.-Y. Choi, M. Suh, J.-G. Kim, I.-H. Suh, J. Chin, *Inorg. Chem. Commun.* **2001**, 377–380; d) P. J. Steel, C. J. Sumby, *Chem. Commun.* **2002**, 322–323; e) G. J. Halder, C. J. Kepert, B. Moubaraki, K. S. Murray, C. S. Cashion, *Science* **2002**, *298*, 1762–1765; f) H. Adams, S. Clunas, D. E. Fenton, D. N. Towers, *J. Chem. Soc. Dalton Trans.* **2002**, 3933–3935; g) D. K. Chand, K. Biradha, M. Fujita, S. Sakamoto, K. Yamaguchi, *Chem. Commun.* **2002**, 2486–2487; h) R. W. Saalfrank, H. Glaser, B. D. B. F. Hampel, M. M. Chowdhry, V. Schunemann, A. X. Trautwein, G. B. M. Vaughan, R. Yeh, A. V. Davis, K. N. Raymond, *Chem. Eur. J.* **2002**, *8*, 493–497; i) P. de Wolf, S. L. Heath, J. A. Thomas, *Chem. Commun.* **2002**, 2540–2541.
[3] Grids, see for example: a) M.-T. Youinou, N. Rahmouni, J. Fischer, J. A. Osborn, *Angew. Chem.* **1992**, *104*, 771–773; *Angew. Chem. Int. Ed. Engl.* **1992**, *31*, 733–735; b) G. S. Hanan, D. Volkmer, U. S. Schubert, J.-M. Lehn, G. Baum, D. Fenske, *Angew. Chem.* **1997**, *109*, 1929–1931; *Angew. Chem. Int. Ed. Engl.* **1997**, *36*, 1842–1844; c) F. J. Romero-Salguero, J.-M. Lehn, *Tetrahedron Lett.* **1999**, *40*, 859–862; d) K. L. V. Mann, E. Psillakis, J. C. Jeffery, L. H. Rees, N. M. Harden, J. A. McCleverty, M. D. Ward, D. Gatteschi, F. Totti, F. E. Mabbs, E. J. L. McInnes, P. C. Riedi, G. M. Smith, *J. Chem. Soc. Dalton Trans.* **1999**, 339–348; e) C. S. Campos-Fernandez, R. Clerac, K. R. Dunbar, *Angew. Chem.* **1999**, *111*, 3685–3688; *Angew. Chem. Int. Ed.* **1999**, *38*, 3477–3479; f) E. Breuning, M. Ruben, J.-M. Lehn, F. Renz, Y. Garcia, V. Ksenofontov, P. Gutlich, E. Wegelius, K. Rissanen, *Angew. Chem.* **2000**, *112*, 2563–2566; *Angew. Chem. Int. Ed.* **2000**, *39*, 2504–2507; g) P. N. W. Baxter, J.-M. Lehn, G. Baum, D. Fenske, *Chem. Eur. J.* **2000**, *6*, 4510–4517; h) L. Zhao, Z. Xu, L. K. Thompson, S. L. Heath, D. O. Miller, M. Ohba, *Angew. Chem.* **2000**, *112*, 3244–3247; *Angew. Chem. Int. Ed.* **2000**, *39*, 3114–3117; i) T. Bark, M. Duggeli, H. Stoeckli-Evans, A. von Zelewsky, *Angew. Chem.* **2001**, *113*, 2924–2927; *Angew. Chem. Int. Ed.* **2001**, *40*, 2848–2851; j) E. Breuning, G. S. Hanan, F. J. Romero-Salguero, A. M. Garcia, P. N. W. Baxter, J.-M. Lehn, E. Wegelius, K. Rissanen, H. Nierengarten, A. van Dorsselaer, *Chem. Eur. J.* **2002**, *8*, 3458–3466; k) E. C. Constable, C. E. Housecroft, B. M. Kariuki, N. Kelly, C. B. Smith, *C. R. Chim.* **2002**, *5*, 425–430; l) L. K. Thompson, *Coord. Chem. Rev.* **2002**, *233/234*, 193–206; m) H. Gang, G. Dong, D. Chun-Ying, M. Hong, M. Qing-jin, *New J. Chem.* **2002**, *26*, 1371–1377; n) Ref. [4].
[4] S. Brooker, S. J. Hay, P. G. Plieger, *Angew. Chem.* **2000**, *112*, 2044–2046; *Angew. Chem. Int. Ed.* **2000**, *39*, 1968–1970.
[5] R. H. Wiley, *J. Macromol. Sci. Chem.* **1987**, *24*, 1183–1190.
[6] F. Abraham, M. Lagrenee, S. Sueur, B. Mernari, C. Bremard, *J. Chem. Soc. Dalton Trans.* **1991**, 1443–1447.
[7] S. Brooker, R. J. Kelly, *J. Chem. Soc. Dalton Trans.* **1996**, 2117–2122.
[8] S. Brooker, R. J. Kelly, G. M. Sheldrick, *J. Chem. Soc. Chem. Commun.* **1994**, 487–488.
[9] S. Brooker, R. J. Kelly, B. Moubaraki, K. S. Murray, *Chem. Commun.* **1996**, 2579–2580.
[10] S. Brooker, R. J. Kelly, P. G. Plieger, *Chem. Commun.* **1998**, 1079–1080.
[11] P. G. Plieger, Ph.D. thesis, University of Otago, New Zealand **1998**.
[12] S. Brooker, P. G. Plieger, B. Moubaraki, K. S. Murray, *Angew. Chem.* **1999**, *111*, 424–426; *Angew. Chem. Int. Ed.* **1999**, *38*, 408–410 and front cover feature.
[13] S. Brooker, T. C. Davidson, S. J. Hay, R. J. Kelly, D. K. Kennepohl, P. G. Plieger, B. Moubaraki, K. S. Murray, E. Bill, E. Bothe, *Coord. Chem. Rev.* **2001**, *216/217*, 3–30.
[14] S. Brooker, D. J. de Geest, R. J. Kelly, P. G. Plieger, B. Moubaraki, K. S. Murray, G. B. Jameson, *J. Chem. Soc. Dalton Trans.* **2002**, 2080–2087.
[15] S. Brooker, *Eur. J. Inorg. Chem.* **2002**, 2535–2547 and front cover feature.
[16] a) S. Brooker, J. Hausmann, Y. Lan, unpublished results; b) J. Hausmann, G. B. Jameson, S. Brooker, unpublished results.
[17] R. Stiller, J.-M. Lehn, *Eur. J. Inorg. Chem.* **1998**, *7*, 977–982.
[18] K. M. Gardinier, R. G. Khoury, J.-M. Lehn, *Chem. Eur. J.* **2000**, *6*, 4124–4131.
[19] V. Goral, M. I. Nelen, A. V. Eliseev, J.-M. Lehn, *Proc. Natl. Acad. Sci. USA* **2001**, *98*, 1347–1352.
[20] B. de Bruin, E. Bill, E. Bothe, T. Weyhermuller, K. Wieghardt, *Inorg. Chem.* **2000**, *39*, 2936–2947.
[21] M. G. B. Drew, V. McKee, S. M. Nelson, *J. Chem. Soc. Dalton Trans.* **1978**, 80–84.
[22] G. Haselhorst, K. Wieghardt, S. Keller, B. Schrader, *Inorg. Chem.* **1993**, *32*, 520–525.
[23] W. J. Geary, *Coord. Chem. Rev.* **1971**, *7*, 81–122.
[24] C. A. Hunter, K. R. Lawson, J. Perkins, C. J. Urch, *J. Chem. Soc. Perkin Trans. 2* **2001**, *5*, 651–669.
[25] A. M. Barrios, S. J. Lippard, *Inorg. Chem.* **2001**, *40*, 1060–1064.
[26] J. E. Andrew, A. B. Blake, *J. Chem. Soc. A* **1969**, 1408–1415.
[27] L. Rosenberg, L. K. Thompson, E. J. Gabe, F. L. Lee, *J. Chem. Soc. Dalton Trans.* **1986**, 625–631.
[28] M. A. A. Miah, D. J. Phillips, A. D. Rae, *Inorg. Chim. Acta* **1992**, *201*, 191–196.
[29] A. Escuer, R. Vicente, B. Mernari, A. E. Gueddi, M. Pierrot, *Inorg. Chem.* **1997**, *36*, 2511–2516.
[30] C. J. Fahrni, A. Pfaltz, M. Neuburger, M. Zehnder, *Helv. Chim. Acta* **1998**, *81*, 507–524.
[31] J. Cano, G. De Munno, F. Lloret, M. Julve, *Inorg. Chem.* **2000**, *39*, 1611–1614.
[32] S. Brooker, J. D. Ewing, J. Nelson, *Inorg. Chim. Acta* **2001**, *317*, 53–58.
[33] S. Brooker, J. D. Ewing, J. Nelson, J. C. Jeffery, *Inorg. Chim. Acta* **2002**, *337*, 463–466.
[34] T. Wen, L. K. Thompson, F. L. Lee, E. J. Gabe, *Inorg. Chem.* **1988**, *27*, 4190–4196.

[35] F. Lloret, G. De Munno, M. Julve, J. Cano, R. Ruiz, A. Caneschi, *Angew. Chem.* **1998**, *110*, 143 – 145; *Angew. Chem. Int. Ed.* **1998**, *37*, 135 – 138.
[36] H.-F. Klein, M. Helwig, U. Koch, U. Florke, H.-J. Haupt, *Z. Naturforsch. B* **1993**, *48*, 778 – 784.
[37] H.-F. Klein, M. Helwig, M. Karnop, H. Konig, B. Hammerschmitt, G. Cordier, U. Florke, H.-J. Haupt, *Z. Naturforsch. Teil B* **1993**, *48*, 785 – 793.
[38] D. Onggo, A. D. Rae, H. A. Goodwin, *Inorg. Chim. Acta* **1990**, *178*, 151 – 163.
[39] P. C. Healy, B. W. Skelton, A. H. White, *Aust. J. Chem.* **1983**, *36*, 2057-.
[40] W. M. Reiff, E. H. Witten, K. Mottle, T. F. Brennan, A. R. Garafalo, *Inorg. Chim. Acta* **1983**, *77*, L83-L88.
[41] M. James, H. Kawaguchi, K. Tatsumi, *Polyhedron* **1997**, *16*, 4279 – 4282.
[42] J. A. Real, G. DeMunno, M. C. Munoz, M. Julve, *Inorg. Chem.* **1991**, *30*, 2701 – 2704.
[43] K. R. Dunbar, J. J. Longridge, J. M. Rawson, J.-S. Sun, *Inorg. Synth.* **2002**, *33*, 103 – 107.
[44] J. L. Sessler, J. W. Sibert, V. Lynch, *Inorg. Chim. Acta* **1994**, *216*, 89 – 95.
[45] F. H. Allen, S. A. Bellard, M. D. Brice, B. A. Cartwright, A. Doubleday, H. Higgs, T. Hummelink, B. G. Hummelink-Peters, O. Kennard, W. D. S. Motherwell, J. R. Rodgers, D. G. Watson, *Acta Crystallogr. Sect. B* **1979**, *35*, 2331 – 2339.
[46] S. Bernès, F. Sécheresse, Y. Jenannin, *Inorg. Chim. Acta* **1992**, *194*, 105 – 109.
[47] H.-L. Sun, B.-Q. Ma, S. Gao, G. Su, *Chem. Commun.* **2001**, 2586 – 2587.
[48] R. L. Carlin, A. J. van Duyneveldt, *Magnetic Properties of Transition Metal Compounds*, Springer, New York, **1977**.
[49] D. M. Kurtz, *Chem. Rev.* **1990**, *90*, 585 – 606.
[50] P. Gütlich, *Struct. Bond.* **1981**, *44*, 83 – 195.
[51] R. Greef, R. Peat, L. M. Peter, D. Pletcher, J. Robinson, *Instrumental Methods in Electrochemistry*, Ellis Horwood, Woking, **1985**.
[52] C. D. Brandt, E. J. L. McInnes, S. Brooker, work in progress.
[53] G. J. Kubas, *Inorg. Synth.* **1990**, *28*, 68 – 70.
[54] G. M. Sheldrick, *Acta Crystallogr. Sect. A* **1990**, *46*, 467 – 473.
[55] G. M. Sheldrick, *Methods Enzymol.* **1997**, *276*, 628 – 641.
[56] G. M. Sheldrick, T. R. Schneider, *Methods Enzymol.* **1997**, *277*, 319 – 343.

Received: March 4, 2003 [F4915]